Alma Mater Studiorum
Università degli studi di Bologna

SCUOLA DI SCIENZE

Corso di Laurea Magistrale in Astrofisica e Cosmologia

Dipartimento di Fisica e Astronomia

Properties of Cosmic Voids in Dark Energy simulations

Elaborato finale

Candidata:
Giorgia Pollina

Relatore:
Chiar. mo Prof. :
Lauro Moscardini
Co-relatore:
Marco Baldi

Sessione III
Anno Accademico 2012/2013

Contents

List of Figures

List of Tables

Sommario

Negli ultimi 15 anni, incrociando i risultati ottenuti attraverso osservazioni e simulazioni numeriche, è stato possibile definire il modello Cosmologico Standard che è essenzialmente basato su due assunzioni fondamentali: la prima è la presenza nell'Universo di un nuovo tipo di particella non relativistica denominata Cold Dark Matter (CDM), che produce le buche di potenziale gravitazionale in cui le strutture possono formarsi, mentre la seconda è l'esistenza di una energia oscura (Dark Energy, DE) che giustifica l'espasione accelerata dell'Universo. La più semplice forma di energia oscura è rappresentata dalla costante cosmologica Λ: i due pilastri su cui si erige il modello cosmologico standard, dunque, sono perfettamente riassunti dal suo acronimo ΛCDM.

Sebbene il modello ΛCDM preveda correttamente la gran parte delle osservazioni disponibili, esso presenta degli annosi problemi di autoconsistenza che non sono ancora stati risolti. Uno dei possibili modi per risolvere questi problemi è costituito dall□introduzione di una nuova tipologia di Dark Energy cosiddetta dinamica, cioè associata ad un campo scalare ϕ la cui densità di energia evolve nel tempo. Inoltre esiste la possibilità, che va sotto il nome di Dark Energy accoppiata e che sarà l'oggetto di questa tesi, che il campo ϕ possa interagire direttamente con la materia in diversi regimi.

I vuoti cosmici sono vastissime regioni nell'Universo caratterizzate da una densità molto minore rispetto alla densità media dell'Universo stesso. Poichè essenzialmente prive di materia al loro interno, queste regioni dovrebbero possedere una dinamica completamente dominata dalla Dark Energy. Per questo motivo si suppone che le loro proprietà siano fortemente legate alla sua natura e che, quindi, i vuoti cosmici rappresentino un laboratorio fondamentare per testare modelli cosmologici che assumono differenti forme di DE.

Questo lavoro di tesi si prefigge l'obiettivo di analizzare le proprietà dei vuoti cosmici trovati nei cataloghi di grandi simulationi cosmologiche di Universo a grande scala. In particolare abbiamo utilizzato un codice pubblico dedicato alla ricerca dei vuoti, ZOBOV (riferimento bibliografico [32]), per costruire dei cataloghi di vuoti a partire dai cataloghi di aloni prodotti dalle CoDECS (riferimenti bibliografici [40] e [47]). Le CoDECS sono al momento simulazioni cosmologiche più grandi che contemplano la possibile interazione tra DE e materia. Abbiamo identificato criteri appropriati alla

creazione di cataloghi di vuoti allo scopo di confrontare le proprietà di questi oggetti in modelli che prevedono la presenza di DE accoppiata con il modello ΛCDM.

La discussione è organizzata come segue: nel capitolo 1 vengono introdotti i concetti basilari su cui si fonda la cosmologia standard e le più importanti proprietà dei vuoti cosmici. Nel capitolo 2 vengono presentate le principali caratteristiche delle cosmologie alternative che assumono una Dark Enegy dinamica. Nel capitolo 3 descriviamo il codice pubblico ZOBOV ed i criteri con cui esso viene impiegato per la creazione dei cataloghi di vuoti. Nel capitoli 4 e 5 discutiamo le proprietà statistiche e geometriche osservate negli oggetti inclusi nei nostri cataloghi, mentre nel capitolo 6 riportiamo un riassunto delle nostre conclusioni.

Abstract

The last decade has witnessed the establishment of a Standard Cosmological Model, which is based on two fundamental assumptions: the first one is the existence of a new non relativistic kind of particles, i. e. the Dark Matter (DM) that provides the potential wells in which structures create, while the second one is presence of the Dark Energy (DE), the simplest form of which is represented by the Cosmological Constant Λ, that sources the acceleration in the expansion of our Universe. These two features are summarized by the acronym ΛCDM, which is an abbreviation used to refer to the present Standard Cosmological Model.

Although the Standard Cosmological Model shows a remarkably successful agreement with most of the available observations, it presents some long-standing unsolved problems. A possible way to solve these problems is represented by the introduction of a dynamical Dark Energy, in the form of the scalar field ϕ. In the coupled DE models, the scalar field ϕ features a direct interaction with matter in different regimes.

Cosmic voids are large under-dense regions in the Universe devoided of matter. Being nearby empty of matter their dynamics is supposed to be dominated by DE, to the nature of which the properties of cosmic voids should be very sensitive.

This thesis work is devoted to the statistical and geometrical analysis of cosmic voids in large N-body simulations of structure formation in the context of alternative competing cosmological models. In particular we used the ZOBOV code (see ref. [32]), a publicly available void finder algorithm, to identify voids in the Halos catalogues extraxted from CoDECS simulations (see refs. [40], [47]). The CoDECS are the largest N-body simulations to date of interacting Dark Energy (DE) models. We identify suitable criteria to produce voids catalogues with the aim of comparing the properties of these objects in interacting DE scenarios to the standard ΛCDM model, at different redshifts.

This thesis work is organized as follows: in chapter 1, the Standard Cosmological Model as well as the main properties of cosmic voids are intro-

duced. In chapter 2, we will present the scalar field scenario. In chapter 3 the tools, the methods and the criteria by which a voids catalogue is created are described while in chapter 4 we discuss the statistical properties of cosmic voids included in our catalogues. In chapter 5 the geometrical properties of the catalogued cosmic voids are presented by means of their stacked profiles. In chapter 6 we summarized our results and we propose further developments of this work.

Chapter 1

Introduction

In this chapter we will present a brief introduction to the main concepts on which the Standard Cosmological Model is based. we will start by introducing the reader to the basic equations that describes the dynamical evolution of the Universe. Then, we will discuss the general properties of cosmic Voids and their application as cosmological probes.

1.1 The Standard Cosmological Model

The challenge to describe the evolution of the Universe is intimately related to the behavior of gravity: in fact, on sufficiently large scales the leading interaction is gravitation. Gravity is described by the theory of General Relativity (GR) developed by Albert Einstein in 1915 (see ref. [1]). Therefore, we am going to set in some primary concepts regarding GR.

1.1.1 The field equations and the Cosmological Principle

In the context of Einstein's theory of GR, the effect of gravity is encoded in the geometry of the space-time described by a metric tensor $g_{\mu\nu}$. The minimum distance between two events in the spacetime (*line element*) is given by:

$$ds^2 = g_{\mu\nu} dx^\mu dx^\nu . \tag{1.1}$$

Let $G_{\mu\nu}$ be the Einstein tensor defined as

$$G_{\mu\nu} \equiv R_{\mu\nu} - \frac{1}{2} R g_{\mu\nu} , \tag{1.2}$$

where $R_{\mu\nu}$ is the Ricci Tensor and the Curvature Scalar R are both defined starting from the Riemann Tensor $R^\sigma_{\lambda\mu\nu}$, as follows:

$$R_{\mu\nu} \equiv R^\sigma_{\mu\sigma\nu} , \tag{1.3}$$

$$R \equiv R^{\nu}_{\nu} = g^{\mu\nu} R_{\mu\nu} \,, \tag{1.4}$$

respectively. The Einstein tensor $G_{\mu\nu}$ returns information about the space-time geometry. The Standard Cosmological Model is based on the Einstein field equation of General Relativity, that reads

$$G_{\mu\nu} = \kappa^2 T_{\mu\nu} \,, \tag{1.5}$$

where:

- $\kappa^2 \equiv 8\pi G$, G being Newton's gravitational constant;
- $T_{\mu\nu}$ is the total stress-energy tensor, which encodes information about the energy distribution in the Universe.

Considering a perfect fluid (in its rest frame), its stress-energy tensor $T_{\mu\nu}$ can be written as follows:

$$T_{\mu\nu} = (\rho + p) u_\mu u_\nu + p g_{\mu\nu} \,, \tag{1.6}$$

where:

- ρ is the energy density of the fluid;
- p is the pressure of the fluid;
- u_μ is the 4-velocity of the fluid element;
- The speed of light c is constant and equal to 1[1] .

The equation of state of a perfect fluid is defined by the ratio between its pressure and energy densities:

$$w \equiv \frac{p}{\rho} \,, \tag{1.7}$$

which lies in the range:

$$-1 \leq w \leq 1. \tag{1.8}$$

The energy content of the Universe can be described in terms of different types of fluid with distinct equations of state. Therefore, the expression for total stress-energy tensor in eq.1.5 will be given by the sum of equations of state of all the fluids:

$$T^{tot}_{\mu\nu} = \sum_i T^{(i)}_{\mu\nu}. \tag{1.9}$$

The values of the equation of state eq. 1.7 of different kinds of fluid in the Universe are:

[1]The speed of light c will be always considered constant and equal to 1 unless specified otherwise.

- for radiation and relativistic matter

$$w_{rad} = 1/3\,; \tag{1.10}$$

- for matter

$$w_{matter} = 0\,. \tag{1.11}$$

These values imply important consequences in the evolution of the Universe, as it will presented in the next section.

Another crucial axiom on which Modern Cosmology stands is the hypothesis that the Universe is homogeneous and isotropic on sufficiently large scale (i.e. on scales greater than $\sim 100Mpc$): basically this means that there are no preferential directions or positions in the Universe. This assumption goes under the name of *Cosmological principle*, and it allows to describe the general form of the metric tensor of the Universe in a simple form, as discussed in the next section.

1.1.2 The Friedmann-Lamaitre-Robertson-Walker metric

As already defined in eq. 1.1 the line element is given by:

$$ds^2 = g_{\mu\nu} dx^\mu dx^\nu .$$

Under the hypotesis of homogeneity and isotropy stated in the Cosmological principle we obtain the maximally-symmetric *Friedman-Lemaitre-Robertson-Walker* (FLRW) metric[2]:

$$ds^2 = dt^2 - a^2(t) \left[\frac{dr^2}{1 - kr^2} + r^2 (d\theta^2 + \sin^2\theta \, d\phi^2) \right] , \tag{1.12}$$

where

- (r, θ, ϕ) are the *comoving coordinates*[3];
- t is the cosmic time;
- $a(t)$ is the cosmic scale factor i.e. a dimensionless function of time which represents the relative expansion of the Universe. The cosmic scale factor describes the global evolution of the Universe;
- k is a parameter that defines the global curvature of the space: it can take $+1$, -1, 0 for a close (spherical), open (hyperbolic), or flat (euclidean) curvature (geometry) of the Universe, respectively.

[2] The sign conventions are the same as ref. [13]

[3] These are the coordinates at rest with respect to the Universe's expansion.

With this metric, the proper distance, d_p, between two events is:

$$d_p = \int_0^r \frac{a\, dr'}{(1 - kr'^2)^{1/2}} = a\, f(r)\,, \tag{1.13}$$

where

$$f(r) = \begin{cases} \sin^{-1}(r), & \text{for } k = 1 \\ r, & \text{for } k = 0 \\ \sinh^{-1}(r), & \text{for } k = -1 \end{cases} . \tag{1.14}$$

Considering two objects in the Universe, their proper distance is related by the scale factor $a(t)$. Using the FLRW metric (eq. 1.12) in the field equations of General Relativity (1.5) it is possible to obtain two evolution equations for $a(t)$ which describe the dynamic evolution of the Universe:

$$\left(\frac{\dot{a}}{a}\right)^2 = \frac{\kappa^2}{3}\left[\rho_k + \sum_i \rho_i\right] , \tag{1.15}$$

$$\frac{\ddot{a}}{a} = -\frac{\kappa^2}{6}\sum_i (\rho_i + 3p_i)\,, \tag{1.16}$$

where:

- ρ_k is the curvature density so that

$$\rho_k \equiv -\frac{3}{\kappa^2}\frac{k}{a^2}\,;$$

- ρ_i and p_i are the energy density and the pressure respectively, of different components of the Universe (baryonic matter, dark matter, neutrinos and radiation);
- $\dot{a}$ and $\ddot{a}$ are the first and the second derivative of the scale factor with respect to the cosmic time, respectively.

Eq. 1.15 can be rewritten in terms of the Hubble parameter, which is defined as

$$H(t) \equiv \frac{\dot{a}}{a}\,, \tag{1.17}$$

in the following way:

$$H^2(t) \equiv \left(\frac{\dot{a}}{a}\right)^2 = \frac{\kappa^2}{3}\left[\rho_k + \sum_i \rho_i\right] . \tag{1.18}$$

Equations 1.15 and 1.16 are known as the *Friedmann equations* and determine the evolution of the Universe with respect to the time.

Matter and radiation can be considered as perfect fluids. Calculating the trace of the stress energy tensor of a perfect fluid it is possible to state the *strong energy condition*:

$$\rho + 3p \geq 0. \tag{1.19}$$

This condition is valid for all fluids in the Universe. Matter fulfills eq. 1.19 with a value greater than zero, because of its equation of state. Therefore, the *Friedmann equations* (1.15 and 1.16) for a combination of fluid that fulfill the *strong energy condition* (eq. 1.19) do not have a static solution, because the second derivative of the scale factor (i.e. $\ddot{a}$) is always negative.

1.2 The Cosmological Costant

The fact that no static solutions for the evolution of the Universe are found by General Relativity induced Albert Einstein, who believed the Universe to be eternal and unchanging, to modify the field eq. 1.5. In the following section we are going to present how this assumption affects the evolution of the Universe.

1.2.1 The introduction of Λ

In order to allow a static solution for the cosmic scale factor a, the field equations of General Relativity were revised, by introducing a Cosmological Constant (Λ) term which balances the attractive pull of gravity.

The Λ term is purely a property of space-time: it has not a dependency on the energy distribution of all the different components which produce the gravitational field of the Universe. Consequently, the Cosmological Constant is most naturally introduced as a modification of the Einstein tensor:

$$\hat{G}_{\mu\nu} \equiv G_{\mu\nu} + \Lambda g_{\mu\nu}. \tag{1.20}$$

It is important to stress that the Cosmological Constant is not a merely hand-made trickery. This term can arise formally as a constant of integration of the theory. In fact, considering the most general action S that it is possible to write in terms of the metric tensor and of its first and second derivatives with respect to the space-time coordinates x^μ,

$$S = \frac{1}{2\kappa^2} \int d^4x \sqrt{-g}(R - 2\Lambda + \mathcal{L}) \,, \tag{1.21}$$

where:

- g is the determinant of the metric tensor;
- $\mathcal{L}$ is the Lagrangian density of all energy fields in the Universe;

- Λ is a constant;

and computing the field equation of eq. 1.21 by means of the *Least Action Principle*, the new field equations of General Relativity can be found:

$$\hat{G}_{\mu\nu} = \kappa^2 T_{\mu\nu} \tag{1.22}$$

being $\hat{G}_{\mu\nu}$ the Einstein tensor defined in eq. 1.20. In the original formulation of GR Λ was assumed to be zero, so that, by integrating eq. 1.21, the early original equations 1.5 are recovered.

1.2.2 The Λ component of the Universe

The Cosmological Constant term can be also interpreted as an additional component of the total stress-energy tensor of the Universe by moving it to the right-hand side of eq. 1.22:

$$G_{\mu\nu} = \kappa^2 \hat{T}_{\mu\nu}, \tag{1.23}$$

where $\hat{T}_{\mu\nu}$ is defined as follows

$$\hat{T}_{\mu\nu} \equiv T_{\mu\nu} - \frac{\Lambda}{\kappa^2} g_{\mu\nu}. \tag{1.24}$$

Under the assumption that the Cosmological Constant is a perfect fluid, it is possible to find the formal energy density and pressure of the Λ term using eq. 1.6:

$$\rho_\Lambda = \frac{\Lambda}{\kappa^2}, \tag{1.25}$$

$$p_\Lambda = -\frac{\Lambda}{\kappa^2}. \tag{1.26}$$

From these last expressions we find the equation of state for Cosmological Constant:

$$w_\Lambda \equiv \frac{p_\Lambda}{\rho_\Lambda} = -1. \tag{1.27}$$

Eq. 1.27 determines the role of the Cosmological Constant in the evolution of the Universe: this result violates the *Strong Energy Condition* (eq. 1.19). Therefore the Friedmann equations becomes:

$$\left(\frac{\dot{a}}{a}\right)^2 = \frac{\kappa^2}{3}\left[\rho_k + \rho_\Lambda + \sum_i \rho_i\right], \tag{1.28}$$

$$\frac{\ddot{a}}{a} = -\frac{\kappa^2}{6}\left[-2\rho_\Lambda + \sum_i (\rho_i + 3p_i)\right]. \tag{1.29}$$

Therefore the Cosmological Constant is able to act against gravity allowing static (although unstable) solutions for $k = +1$ and non negative values of ρ_i, p_i, and Λ.

In 1929, however, Edwin Hubble discovered the expansion of the Universe (ref. [2]) and the introduction of a static solution for the Friedmann's equations did not seem like a possible outcome anymore. The Cosmological Constant idea was abandoned.

Every now and then the interest in a Λ component renewed. In particular when the acceleration in the expansion of Universe was discovered in 1998 by studies made by the *Supernova Cosmology Project* (see ref. [20]) and the *High-z Supernova Search Team* (ref. [21]) the Cosmological Constant was reintroduced.

In fact, studying the relation between redshift, z, (defined as $z \equiv a^{-1} - 1$) and magnitude for the Supernovae of Type Ia (SN Ia), it is possible to constrain the deceleration parameter[4] q_0, which is defined as:

$$q_0 \equiv \left(\frac{\ddot{a}\, a}{\dot{a}^2} \right)_0 = \left(-\frac{\dot{H} + H^2}{H^2} \right)_0 . \tag{1.30}$$

An evolution of SN Ia magnitude with respect to the redshift z as the one found in ref. [20] and [21]), is incompatible with a decelerating expansion of Universe. The q_0 parameter is constrained by these observation to be negative.

At the end of section 1.1.2 we have already pointed out that all cosmic fluids, whose equation of state satisfies the *Strong Energy Condition* (eq. 1.19), cannot result in a positive value for $\ddot{a}$, and therefore can not determine a negative value of q_0.

A negative value of q_0 like the one found in the *Supernova Cosmology Project* and in the *High-z Supernova Search Team* shows the necessity to consider a fluid in the Universe which does not fullfil eq. 1.19. Therefore the simplest possibility is to consider the Cosmological Constant to be the component which drives the accelerated expansion of the Universe.

Thanks to its equation of state, eq. 1.27, Λ's energy density does not dilute with the expansion of the Universe. In fact for a bariotropic fluid (such that $-1 \leq w \leq +1$) as the Cosmological Constant, it can be found that the energy depends on the scale factor $a(t)$ as written in this relation:

$$\rho_i \propto a^{-3(1+w_i)}. \tag{1.31}$$

Since for the Cosmological Constant $w_\Lambda = -1$ (as stated in eq. 1.27), it is simple to conclude that:

$$\rho_\Lambda = const, \tag{1.32}$$

[4]The subscript 0 indicates that the today's value is considered ($z = 0$).

as already stated by eq. 1.25.

The Cosmological Constant Λ is a possible form of *Dark Energy*. The two pillars on which the Standard Cosmological Model is based, are the cosmological constant Λ (which determines the accelerated expansion of the Universe), and a new kind of non relativistic massive particles named of Cold Dark Matter (CDM) that provide the gravitational potential wells in which cosmic structures form (see **??**). From this two fundamental features comes the acronym ΛCDM that we will use with reference to the Standard Cosmological Model.

In the ΛCDM picture the energy density of the Cosmological Constant, i.e. the (*Dark Energy*) density, has the same value at all cosmic times, and today it drives the accelerated expansion of the Universe. In the next chapter we will present fundamental problems related to eq. 1.32 and how it is possible to challenge the assumption stated by this last cited equation.

1.3 General properties of voids

The Cosmological Principle stated in section 1.1.1, whose assumption is fundamental in order to study the general evolution of the Universe, is violated at small scale, allowing the growth of density perturbation for gravitational instability.

In fact, in the Standard Cosmological Model structures form in a hierarchical process starting from primordial fluctuations in the density distribution of the Universe, ref. [13]. The existence of primordial anisotropies was confirmed for the first time by the observation of fluctuations in the temperature distribution of the Cosmic Microwave Background (CMB), measured by COBE (COsmic Background Explorer), see ref. [14]. The observations show that (ref. [8], [14]):

$$\langle \left(\frac{\delta T}{T} \right)^2 \rangle^{1/2} \equiv \frac{T(\theta, \phi) - \langle T \rangle}{\langle T \rangle} \approx 10^{-5}, \tag{1.33}$$

where:

- $T(\theta, \phi)$ is the CMB temperature distribution, being θ and ϕ the angular coordinates;
- $\langle T \rangle$ is the mean temperature, today mesured $T = 2.73K$

Since in the Early Universe matter and radiation were coupled via Thomson scattering, fluctuations in the temperature distribution imply the existence of an inhomogeneous distribution of density, so the birth of structures is due to the gravitational instability process acting on primordial density

fluctuations. In first approximation we can picture the densities perturbation as a Gaussian random field. The amplitude of such perturbations is able to grow under a collapse due to self-gravity.

The generation of the *Cosmic Web* from primordial fluctuations is a natural outcome of the gravitational anisotropic collapse (see ref. [3]). The term "Cosmic Web" comes originally from the visual inspection of the outcomes of cosmological simulations which reproduce the distribution of Dark Matter (DM) in the Universe. Galaxies, which follow the DM distribution, are arranged in clusters joined by elongated filaments while voids are large under-dense regions nestled in the Cosmic Web (see ref. [19]). Voids are believed to originate from negative density fluctuations in the primordial density field (see re. [**?**]). As a result of their under-density they dynamics is dominated by the DE

The presence of voids in the large scale structures distribution of galaxies is one of the earliest predictions of the CDM scenario (see ref. [9]), and their first discovery in a galaxy survey is now an important tassel in modern Cosmology (see ref. [5] and [7]).

Since their first discovery, properties of voids have been studied for years but only recently, due to the increasing depth and volume of current galaxies surveys, it has been possible to make systematic studies about these large under-dense regions (see ref. [25]). Voids are now one of the most relevant feature in the large scale structure of the Universe. Although a widespread and universal definition of cosmic void does not exists, thanks to a combination of results obtained from simulations and observations, we now have a coherent picture of voids properties in the ΛCDM scenario.

Voids can be describe in first approximation as large spheres with (see ref. [43]):

- typical radius $R_{voids} \approx 10 - 40\, Mpc$;
- typical density $\rho_{voids} \lesssim 0.1 - 0.2\, \rho_{mean}$, where ρ_{mean} is the mean density of the Universe.

The results of the observations provided by many surveys, as for example the Void Galaxy Survey (ref. [39]) and the Las Campana Redshift Survey (ref. [24]) have confirmed that voids are the dominant volume filling component in the Universe.

The radial density profile of a void in spherical approximation is shaped as a central under-density, which due to mass conservation must be compensate: in fact at $R \sim R_{void}$ a minor over-density is expected to be shown. On the other hand, at large radii, a density similar to the mean density of the Universe should be found (see ref. [53]), since the Universe is expected to be homogeneous and isotropic as stated by the Cosmological Principle (see sec 1.1.1). In fig. 1.2 We report an example of density profile found in literature (ref. [46]).

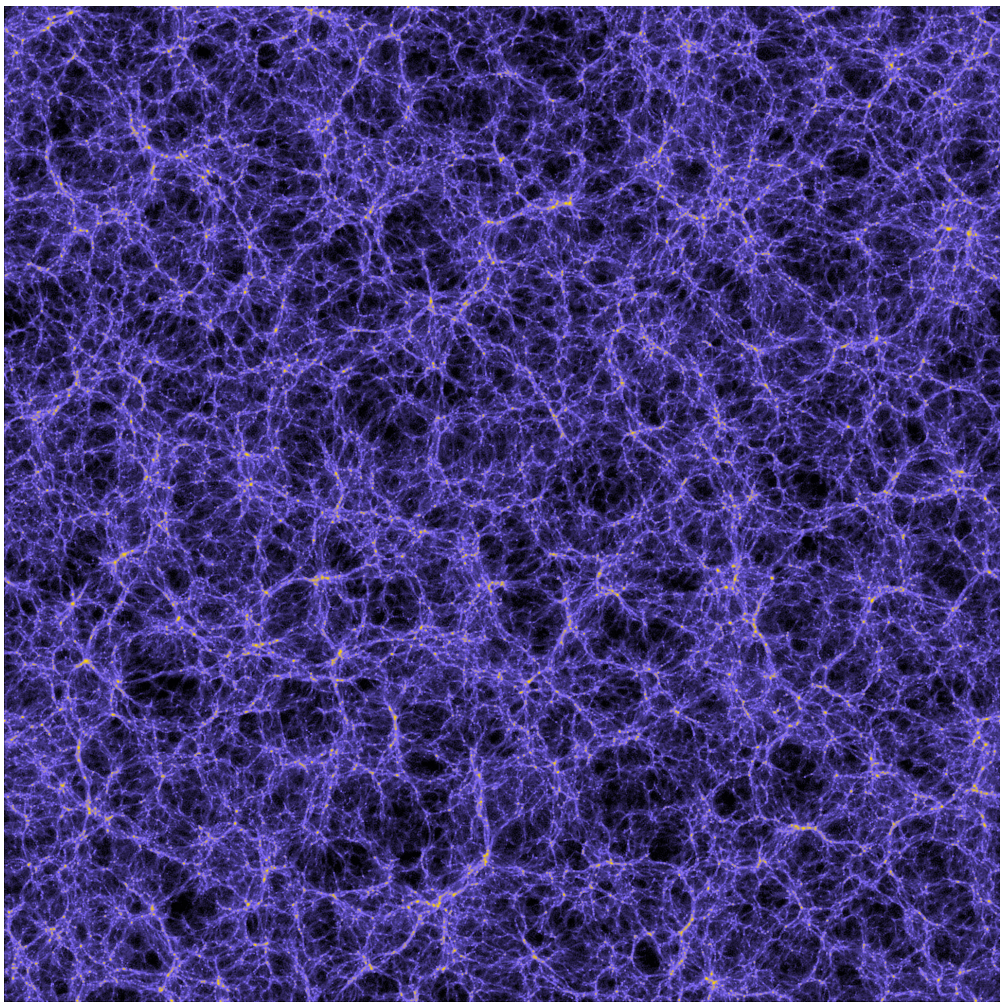

Figure 1.1: A snapshot from the cosmological N-body simulations CoDECS (which will be described in the next chapter). The slice visualized has dimensions $1000 \times 1000 \times 30 Mpc/h$ (where h is the the parameter which allows to rescale H) and reproduces the distribution of CDM in ΛCDM scenario at $z = 0$. It is possible to appreciate how CDM (whose distribution is followed by baryons) builds a net, the Cosmic Web, while voids are nestled within filaments and clusters.

Recent studies have investigated the properties of stacking voids. The stacking is a procedure that computes a mean density profile of several voids with comparable size (ref. [46]), with the aim to constrain cosmological parameters (ref. [41]) or to test modify gravity (ref. [48]). As long as voids are nearly empty of matter, their dynamic is dominated by Dark Energy (DE): they are subject to an effective repulsive pull causing their expansion. As a consequence of such expansion, the matter within the voids evacuates from the interior and accumulates to the boundaries. This feature leads to the void density profile observed in fig. 1.2.

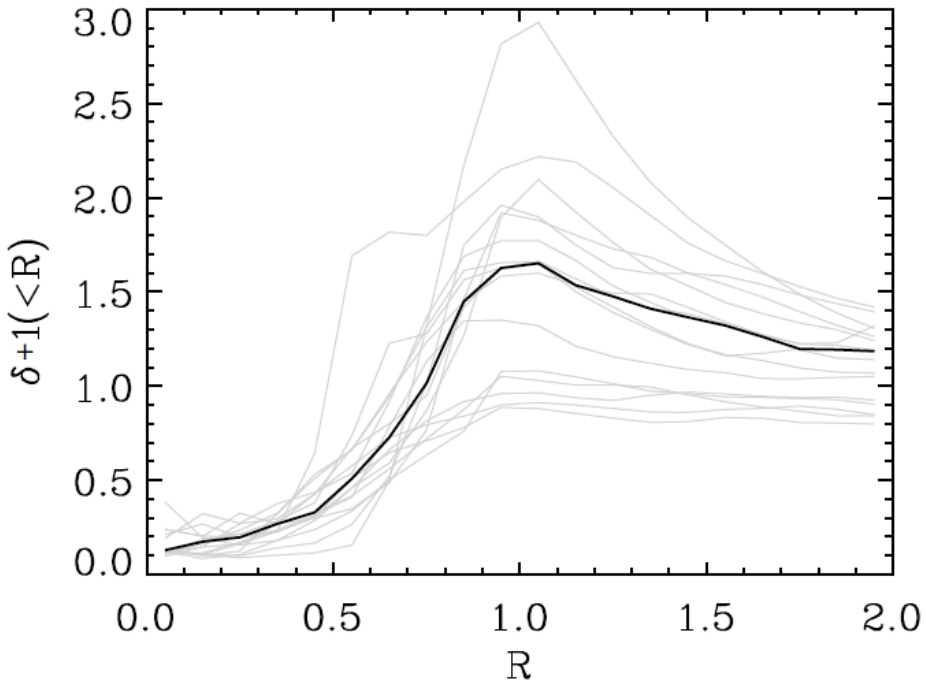

Figure 1.2: Radial density profiles of voids found in a N-body simulation as function of radius, which was calculated within spheres with increasing radii and placed at the center of the void. The black line is the mean (stacked profile) of all the grey profiles everyone of which refers to a single void. In this case (see ref. [46]) the x-axis is scaled so that the density profile for each void has its peak at $R = 1$.

As already pointed out Λ is a possible form of Dark Energy. In section 2.2 it will be presented another possible form of Dark Energy: the dynamical DE which is associated to a scalar field ϕ. The *Quintessence* and the *coupled Dark Energy* scenarios both assume the presence of dynamical DE with different coupling regime: a weak coupling regime for the former (i.e. the scalar field ϕ does not exchange energy with other fluids in the Universe) and a strong coupling regime for the latter (i.e. the scalar field ϕ is allowed to interact with other components in the Universe). Since the dynamic of cosmic voids is dominated by DE the analysis of their properties of voids can be of use to study the differences between these models.

The goal of this work is to investigate statistical and geometrical properties of cosmic voids in different cosmological scenarios.

Chapter 2

Dark Energy

Although ΛCDM is the model of reference in Cosmology, it presents some longstanding problems that have not been solved yet. The unresolved issues of ΛCDM represent the main motivation for the investigation of new Cosmological scenarios.

As we have already mentioned at the end of the previous chapter, two theories (which are characterized by a different explanation for the accelerated expansion of the Universe with respect to ΛCDM) are challenging the Standard Cosmological Model: the *Quintessence* and the *coupled Dark Energy*. Both of these theories introduce a scalar field ϕ, by means of which it is possible to explain the expansion of the Universe. In fact the former theory introduces a time dependency in the dark energy density ρ_ϕ by means of a scalar field ϕ , while the latter assumes that not only ρ_ϕ has a time dependency, but also that the scalar field ϕ can interact with the Dark Matter.

In this chapter we are going to present the some of the most important features of the scalar field scenario.

2.1 Problems of ΛCDM

As presented in Chapter 1, the Standard ΛCDM model is today the model that presents the best agreement with observations, and, consequently, is considered the point of reference in Cosmology. However, the model presents three major problems, which are worth being briefly discussed:

(i). The cosmological constant problem;

(ii). The fine tuning problem;

(iii). The coincidence problem;

2.1.1 The Cosmological Constant problem

As already mentioned in section 1.2.2, the introduction of Λ entails the presence in the Universe of a new component whose energy density is constant in time (see eq. 1.25) and does not dilute with the expansion of the cosmic volume (eq. 1.32). In particle physics, the zero point energy of the Quantum Field Theory (QFT) has also the property of not diluting with the volume; in fact the expectation value of the stress-energy tensor in the vacuum is given by:

$$T_{\mu\nu}^{(vac)} = \rho_{vac} g_{\mu\nu} \,, \tag{2.1}$$

where ρ_{vac} is the energy density of the vacuum. By comparing the last equation and eq. 1.6 it is possible to conclude that the pressure density of the vacuum is $p_{vac} = -\rho_{vac}$ which means that its equation of state is $w_{vac} = -1$, exactly like Λ (eq. 1.27). The expression for the stress energy tensor of the vacuum, eq. 2.1, is the same that appears if Λ is treated as a perfect fluid in eq. 1.20, so that, in analogy with the consideration made for Cosmological Constant, we can conclude:

$$\rho_{vac} = \rho_\Lambda = \frac{\Lambda}{8\pi G}. \tag{2.2}$$

Due to all the mentioned analogies between vacuum and Λ fluids, the zero point energy of QFT has been considered as a candidate to explain Λ's feature. It is possible to compute the energy density of the vacuum, which should predict the value of ρ_Λ observed today. The energy density of the vacuum is calculated by the integral in momentum space of the zero-point energy of the quantuum fields up to a fixed energy, k^*, which is chosen to be the Planck energy $k_{Pl} = \sqrt{(\hbar c^5)/(G)}$. However, following this last line of reasoning it is possible to show that the observational value of the energy density of Λ, ρ_Λ^{obs} is many order of magnitude smaller than the predicted one, ρ_Λ^{th} (see ref. [12]).

The discrepancy is huge:

$$\rho_\Lambda^{th} \sim 10^{123}\, \rho_\Lambda^{obs} \,, \tag{2.3}$$

and this has being called the worst prediction in the history of physics.

2.1.2 The fine tuning problem

Thanks to eq. 1.31

$$\rho_i(w) = a^{-3(1+w_i)} \,,$$

it is possible to compute the dependency of the energy density with respect to the scale factor for all of the components, i, present in the Universe (if the equation of state

$$w_i \equiv \frac{\rho_i}{p_i}$$

of each fluid i is known).

The values of w_i are:

$$w_i = \begin{cases} 0 & \text{for the matter} \\ 1/3 & \text{for the radiation} \\ -1 & \text{for } \Lambda \end{cases} . \tag{2.4}$$

Substituting the w_i values in eq. 1.31 the evolution of the energy density of each fluid with respect to a is found. The results are reported in fig. 2.1, from which it is neat that the energy density of Cosmological Constant was sensibly smaller than energy density of other fluids in the Universe in very remote past.

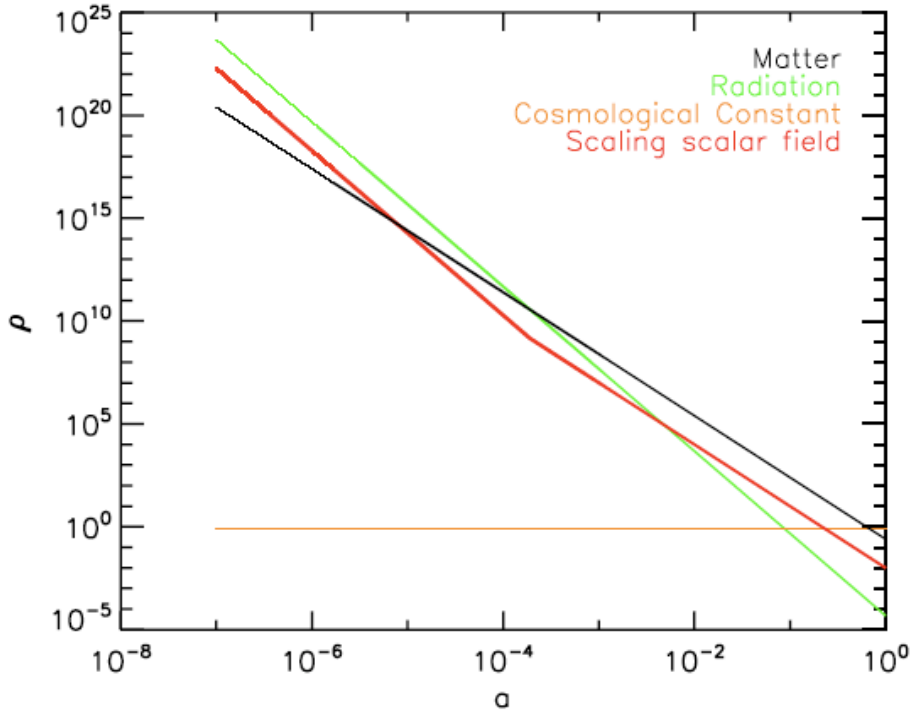

Figure 2.1: Evolution with the scale factor a of the logarithm of energy density ρ of each fluid (figure from ref. [34]). Matter (black line) and radiation (green line) scale respectively as a^{-3} and a^{-4}, while the Cosmological Constant (orange line) has a energy density value constant for all epochs. The red line shows the scaling solution, which will be discuss in sec. 2.2.1. From this plot it is possible to appreciate that ρ_Λ had a very smaller values than other component looking at very early times; nevertheless, ρ_Λ has started to dominate the expansion of the Universe in a very recent past.

It is possible to compute the value of ρ_Λ at the Planck time

$$t_{Pl} \simeq \left(\frac{\hbar G}{c^5}\right)^{1/2} \simeq 10^{-43}\, s\,, \tag{2.5}$$

where $\hbar$ is the Planck constant. The value of ρ_Λ at $t = t_{Pl}$ turns out to be 10^{123} times[1] smaller than other fluids component contributions.

This discrepancy shows that the time-independency of Λ does not appear like a solid hypothesis.

2.1.3 The Coincidence problem

Last but not least, the coincidence problem concerns the fact that Cosmological Constant starts to dominate the expansion of Universe in a very recent past (see fig. 2.1).

As we have already pointed out several times, the expansion of the Universe does not effect the energy density of Λ , which is always constant (see eq. 1.25). On the other hand, the energy density of matter drops in inverse proportion to the volume. So there is only one single moment of cosmological time in which the contribution of dark energy density and energy density of matter are allowed to be of comparable magnitudes. It is possible to argue that to be living in that moment is too unlikely to be coincidence.

For ΛCDM scenario this coincidence is constrained by the measured value of energy density of Cosmological Constant, which means that this problem is equivalent to the fine tuning problem. Nevertheless, in other theories, like those that be presented in the next section, these two problems differ.

2.2 Extending the Standard Model

In order to solve the problems which were enumerated in section 2.1, we need to find a way to:

- Let ρ_Λ be time dependent;
- Find a physical reason why Λ is now dominating the expansion of Universe.

In this section we will discuss the possibility to associate the Dark Energy to a scalar field ϕ, with the aim to challenge the ΛCDM picture. We will present two possible scenarios: in the first ϕ is minimally coupled (i.e. it interacts with itself only), while in the second ϕ is strongly coupled (i.e it is allowed to interact with another field of the Universe).

[1] The fact that this factor is equal to the one appeared in section 2.1.1 does not mean that we are talking about the same problem. The value is the same because we took the Planck energy and the Planck time as a limit in both cases.

2.2.1 Quintessence field with a SUGRA potential

The first solution one can think about in order to solve some of the problems presented by ΛCDM is to introduce a dependency on time of the Dark Energy. The simplest method to do that is based on the introduction of classical[2] self-interacting scalar field, ϕ, with which a potential, $V(\phi)$, is associated.

The scalar field that describes the evolution with time of the DE density was introduced for the first time in 1988 by Christof Wetterich (ref. [10]) who named it *Cosmon*. A couple of months later a similar work written by Ratra & Pleebles (ref. [11]) was published, in which the scalar field was called *Quintessence*.

It is possible to find the *Klein-Gordon equation* for ϕ

$$\ddot{\phi} + 3H\dot{\phi} + \frac{dV}{d\phi} = 0, \tag{2.6}$$

and, considering the Ratra-Pleebles (see ref. [11]) potential

$$V(\phi) \propto e^{-\alpha\phi}\,, \tag{2.7}$$

or an exponential potential

$$V(\phi) \propto \phi^{-\alpha}\,, \tag{2.8}$$

it is possible to find the so called *tracking solutions* (or *scaling solutions*) for the DE (see ref. [34]). These are solutions along which the DE density always evolves as the dominant component in the Universe. The red line in fig. 2.1 shows the evolution of the DE density (to which, in the context of Quintessence, we will refer as ρ_ϕ) for a scaling solution. As it is possible to appreciate in the same figure, scaling solutions let ρ_ϕ evolve with time, giving it the possibility to behave similarly to other components at t_{Pl} and to lately decrease.

However, in this picture the DE density always has a lower contribution than the dominant component (see fig. 2.1). In fact observational constraints set an upper limit on the ratio between the early dark energy density and the total energy density of the Universe Ω_{EDE}:

$$\Omega_{EDE} \leq 2.3 \times 10^{-2}\,, \tag{2.9}$$

calculated at the last scattering surface (see ref. [35]). Thereby DE must be subdominant during the whole radiation dominated epoch and for the greatest part of the matter dominated epoch without exceeding a few percent of the total energy density. On the other hand contribution of ρ_ϕ that we observe today is $\sim 75\%$ of the total energy density of the Universe. In

[2] A *Classical Scalar Field* is a physical entity whose behavior at any point of the space time is completely explained by a single number.

conclusion, since in the *Quintessence* scenario the DE density evolution always follows the fluid that drives the expansion of the Universe and it is constrained to always have a contribution lower than the one of the dominant fluid, it is impossible for the Dark Energy to start being the dominant component (which is what we observe today).

A first strategy to solve this discrepancy is to introduce a new, not monotonically decreasing, potential. Such a potential would allow solutions similar to the tracking solutions at early times but should let the DE density increase after a minimum, justifying its dominance today. The *SUper GRAvity* potential[3] (SUGRA), introduced by Brax and Martin in 1999 (ref. [22]), has the following proportionality:

$$V(\phi) \propto \phi^{-\alpha} e^{\frac{\phi^2}{2}} , \tag{2.10}$$

which fulfills the desired trend of the solution. The SUGRA potential, in fact, behaves as follows:

$$\begin{cases} V(\phi) \to \phi^{-\alpha} & \text{for } \phi \to 0 \\ V(\phi) \to e^{\frac{\phi^2}{2}} & \text{for } \phi \to \infty . \end{cases} \tag{2.11}$$

Thanks to its behavior described in eq. 2.11, the SUGRA potential reproduces the Ratra-Pleebles potential for small values of ϕ allowing the presence of the tracking solutions at early times; on the other hand, for large values of ϕ, tracking solutions are no longer present: in this regime the term $e^{\frac{\phi^2}{2}}$ strongly perturb the Ratra-Peebles potential and the SUGRA potential undergoes an increasing trend which allows solutions to positively grow. Therefore it is now possible for the DE component to "exit" from the evolutionary tracks made by other fluids and to start dominating the expansion of the Universe.

Unfortunately, nothing about *when* should this happen is stated by the shape of SUGRA-potential solutions. Once again, the "exit" needs to be tuned by hand, in order to reach the required consistency with observations. Thus, not all issues of ΛCDM find a solution in this scenario: **SUGRA's picture solves the fine-tuning problem** (see section 2.1.2) **but the problem of Coincidence** (which is now distinct from the fine-tuning problem, see section 2.1.3) **persists.**

2.2.2 Coupled Dark Energy

As we have just mentioned Quintessence and its scaling solutions fail to produce an elegant way in which DE starts driving the expansion of the Universe. Formally this happens because the solution found for eq. 2.6 appears to be

[3]Such hypothesis is introduced by Super Symmetry theories that include gravity, from which the definition Super Gravity.

stable in phase space (ref. [34]). A possible way to address this problem is to find a meta-stable solution (a saddle point) so that DE component is able to "exit" the tracking solutions on its own. The challenge to create a model in which the DE behavior fits observations much more naturally finds a good candidate in *coupled Dark Energy* (cDE) models.

Introducing a coupling

The *Quintessence* models replace the Cosmological Constant with a scalar field in order to find a solution to the longstanding problems of the Standard Cosmological model. The introduction of a scalar field produces interesting results: DE energy density evolves in a much more natural way. Nevertheless, a *fine-tuning* issue persists, which is now addressed to the problem of Coincidence: the moment in which the DE crossover occurs needs to be tuned "by hand".

One of the possible way to extend the scalar field scenario consists in assuming that ϕ can directly interact with other fields in the Universe.

As already mentioned in eq. 1.21, the most general action in General Relativity (without the Λ-term) is given by:

$$S = \frac{1}{2\kappa^2} \int d^4x \sqrt{-g}(R + \mathcal{L}) \,, \tag{2.12}$$

where a gravitational (or curvature) term and a Lagrangian term appear. There scalar field can be coupled (i.e. interacts) with other components by means of two methods:

1. The curvature term has a dependence on a scalar degree of freedom ϕ (*Jordan frame*) i.e. ϕ represents another term to be consider in curvature, so the Jordan frame is a modify gravity model;

2. The matter has a dependence with ϕ (*Einstein frame*), i.e. Dark Energy interacts with matter.

It can be shown that these two options are the same under a transformation of the metric. So both of these pictures predict an interaction between DE and matter. Nevertheless this interaction was constrained by experiments run in the Solar System to test the laws of gravity (see ref [30]), which found the coupling to baryonic matter (i.e. the ordinary matter in the Universe) to be very small.

There are two modifications by which these constraints can be evaded by theories: either we consider the coupling inefficient when densities are large (as it happens in the Solar Systems) or we claim that the coupling is strong for Dark Matter and weak for baryons (of which Solar System is basically composed). The former hypothesis, named *screening mechanism*, is chosen in the Jordan-frame while the latter (*non-universal coupling*) is considered in the Einstein-frame. In this thesis work Einstein-frame numerical models will be used, so in next section we are going to examine this scheme.

Einstein-frame

Every general-relativistic theory needs to be covariant, which means that the *Contracted Bianchi Identities*:

$$\nabla_\mu G^\mu_\nu = 0 \tag{2.13}$$

(where $G_{\mu\nu}$ is the Einstein tensor) have to be verified (ref. [4]).

From the field equation of General Relativity 1.5 we know that

$$G_{\mu\nu} = k^2 T_{\mu\nu}\,,$$

being $T_{\mu\nu}$ the **total** stress-energy tensor.

From eq. 2.13 and 1.5 we can easily conclude that:

$$\nabla_\mu T^\mu_\nu = 0. \tag{2.14}$$

The properties shown in eq. 2.14 has to be verified by every general-relativistic theory.

Introducing a coupling (C_ν) means defining a component for which $\nabla_\mu T^{(\phi)\mu}_\nu = C_\nu$, with $C_\nu \neq 0$: the only chance to leave the condition 2.14 unviolated is supposing that another fluid i fulfills the condition $\nabla_\mu T^{(i)\mu}_\nu = -C_\nu$ so that the two terms compensate.

This is exactly what is supposed by the coupled Quintessence scenario, which can be summarized as follows:

$$\begin{cases} \nabla_\mu T^{(\phi)\mu}_\nu = C_\nu \\ \nabla_\mu T^{(c)\mu}_\nu = -C_\nu \\ \nabla_\mu T^{(b)\mu}_\nu = 0\,, \end{cases} \tag{2.15}$$

where $T^{(\phi)\mu}_\nu$, $T^{(c)\mu}_\nu$ and $T^{(b)\mu}_\nu$ are the stress-energy tensors of DE, CDM and baryons respectively, so that eq. 2.14 is still valid[4].

Looking at the time evolution of the system ($\nu = 0$), the coupling C_ν is settled using a coupling function $\beta_c(\phi)$:

$$\beta_c(\phi) \equiv \sqrt{\frac{3}{2}} M_{Pl} C_\nu \tag{2.16}$$

(where $M_{Pl} \equiv 1/\sqrt{8\pi G}$ is the Plack mass) and it is possible to find the Klein-Gordon equation

$$\ddot{\phi} + 3H\dot{\phi} + \frac{dV}{d\phi} = \sqrt{\frac{2}{3}}\beta\,\rho_c\,, \tag{2.17}$$

[4]The choice to assume a vanishing baryonic coupling is not the only possible but it is the one of interest for this work. The assumption is the same that is considered by the numerical models used in this thesis work, which, as it will be introduced in the next section, are willing to investigate the effects of a possible coupling between DE and CDM.

that now has a second non-zero member (being ρ_c the DE density).

The continuity equation[5] for CDM presents a modification due to the coupling too:

$$\dot{\rho}(\phi)_c + 3H\dot{\phi} + \frac{dV}{d\phi} = \sqrt{\frac{2}{3}}\rho_c \,. \tag{2.18}$$

Thanks to equation eq. 2.18, it is possible to appreciate that the energy density of the CDM ρ_c no longer fulfills eq. 1.31 but evolves differently to baryonic component:

$$\begin{cases} \rho_c \propto a^{-3}\, m_c(\phi) & \text{for CDM} \\ \rho_b \propto a^{-3} & \text{for barions} \end{cases}, \tag{2.19}$$

where $m_c(\phi)$ is the mass of CDE (that now has a dependency from the field ϕ due to their interaction) and ρ_b is the energy density of the baryons. In fact eq. 2.18 has a second non-zero member and, consequently, the integration of the equation implies the existence of a new term:

$$m_c(\phi) = a^{-\int \beta\dot{\phi}dt} \,. \tag{2.20}$$

Thus, coupling implies exchange of energy between CDM and DE. Furthermore the phase space analysis for the coupled DE picture leads to the conclusion that the coupling scenario produces the meta-stable solution we were looking for in order to find a graceful exit of ϕ from the tracking solution (ref. [34]).

2.2.3 Consequences of coupling

By means of modifications which are introduced in fundamental equations such as eq. 2.17 and 2.18, the coupling scenario leads to several important new outcomes.

The majors consequences of introducing a coupling are the following:

1. As it is stated in eq. 2.19, **the energy density of CDM does not scale with the reciprocal of the volume** because its mass changes due to the interaction with DE.

2. **The fractional Dark Energy density Ω_ϕ term has a dependency on the coupling function**. The new value of Ω_ϕ modifies the calculation of total density parameter:

$$\Omega_{tot} = \Omega_{rad} + \Omega_c + \Omega_b + \Omega_\nu + \Omega_\phi, \tag{2.21}$$

[5] A continuity equation is an equation that describes the transport of a conserved quantity. Continuity equations are local form of conservation priciples.

where Ω_{rad}, Ω_ν, Ω_c and Ω_b are the fractional energy density of radiation, neutrinos, CDM and baryons respectively. By means of the new value of the DE contribution, in eq. 2.21, all other values (Ω_{rad}, Ω_ν, Ω_c and Ω_b) change. In order to match these new numerical contributions to observations it is necessary to allow our Universe to undergo a transient stage named ϕ Matter Dominated Epoch (ϕMDE) at the present time. In ϕMDE the expansion is already accelerated but DE has not reached its maximum pull yet. It is also possible to evaluate that:

$$\Omega_{\phi MDE} = \frac{2}{3}\beta^2 \tag{2.22}$$

(see ref. [37]).

3. **Perturbation evolution is modified: ϕ interacts with CDM introducing a fifth force and a new friction term.** The study of the density perturbation evolution according to linear perturbation theory for the coupling models has determined two relevant effects which directly influence the evolution of structures (ref. [23], [27]). The dynamic equation for CDM density perturbations δ_c in interacting DE scenarios, see ref. [36]

$$\ddot{\delta_c} + (2H - \beta\dot{\phi})\dot{\delta_c} - \frac{3}{2}H^2[(1 + 2\beta^2)\Omega_c\delta_c + \Omega_b\delta_b] = 0 \tag{2.23}$$

(where δ_b is the density perturbation of baryons) displays, in fact, an effective enhancement of the gravitational pull for CDE perturbations by the factor $(1 + 2\beta^2)$ which is known as *fifth force*. Nevertheless, also an additional friction term is shown in eq. 2.23, which is directly proportional to the coupling $-\beta\dot{\phi}\dot{\delta_c}$.

These new features have to be tested thanks e.g. to numerical simulations like the CoDECS set, which will be described in the next section.

2.3 The CoDECS project

Coupled Dark Energy Cosmological Simulations (CoDECS, see ref. [40], [47]) represent the largest suite of publicly available cosmological and hydrodynamical N-body simulations to date featuring a direct interaction between DE and CDM.

An N-body simulation is, in general, a numerical simulation of a dynamical system of particles and it has the advantage to produce results which do not need to be re-process with data reduction before analysis, because no instrument of detection is involved.

In cosmology, the interest in N-body simulation is related to the study of structure-formation processes which lead to the formation of e.g. filaments and clusters of galaxies. Since results of a cosmological simulation can

be compared both with observations and (if possible) with analytical predictions, they are an important tassel, by which new cosmological outcomes can be tested.

This thesis work is devoted to study cosmic voids in the CoDECS, comparing the Standard Model with interacting DE models with different couplings.

The theoretical background in which the CoDECS project is settled is explained in sections 2.2.1 and 2.2.2. In table 2.1 are reported the set of cosmological parameters at $z = 0$ used in these simulations.

Table 2.1: List of CoDECS cosmological parameters, which refer to the results of WMAP7.

Parameter	Value
H_0	$70.3\, km\, s^{-1}\, Mpc^{-1}$
Ω_{CDM}	0.226
Ω_{DE}	0.729
A_s	2.42×10^{-9}
Ω_{bar}	0.0451
n_s	0.966

Besides ΛCDM, the range of models which are contemplated by the CoDECS set differs for the choice of the self-interacting DE potential and for the different coupling functions, $\beta(\phi)$. In particular the potentials used are the ones in eq. 2.7 and 2.10. The coupling function of the CoDECS is defined as follows:

$$\beta_c(\phi) \equiv \beta_0\, e^{\beta_1\, \phi}\,, \tag{2.24}$$

so basically the parameter α, β_0 and β_1 are what changes from a model to another.

In table 2.2 the values of these parameters are reported.

Table 2.2: Lists of CoDECS models and their parameters.

Model	Potential	α	β_0	β_1
ΛCDM	$V(\phi) = A$	$-$	$-$	$-$
EXP001	$V(\phi) = Ae^{-\alpha\phi}$	0.08	0.05	0
EXP002	$V(\phi) = Ae^{-\alpha\phi}$	0.08	0.1	0
EXP003	$V(\phi) = Ae^{-\alpha\phi}$	0.08	0.15	0
EXP008e3	$V(\phi) = Ae^{-\alpha\phi}$	0.08	0.4	3
SUGRA003	$V(\phi) = A\phi^{-\alpha}e^{\phi^2/2}$	2.15	-0.15	0

Many works have investigated the properties of the cosmic structures which are produced by the CoDECS simulations e.g. studying their correlation function (see ref [51]) or their halo mass accretion history (ref. [49]).

This thesis aims at investigating the differences in voids properties that arise due to the new kind of evolution predicted by non-standard models (see section 2.2.3) which are numerically simulated by the CoDECS.

Chapter 3

Methods

In this chapter we will briefly describe the publicly available ZOBOV algorithm and how it was used to build the voids catalogues from the CoDECS simulations.

This chapter is organized as follows: in section 3.1 we will describe the way in which the algorithm works; in section 3.2 we will show the results provided by ZOBOV on a simple test case and in section 3.3 we are going to display the criteria which were developed in order to build the final catalogues.

3.1 ZOBOV - A parameter free void finder

ZOBOV (ZOnes Bordering On Voidness) is a publicly available code (see ref. [32]) that finds density depression in a set of points, preferably given by simulations of large scale structure of Universe[1].

This code aims to find voids, starting from a position file[2], with as few restriction as possible. In fact, the algorithm is parameter free and it can be run without setting any constant (although it is possible to introduce a density threshold, useful for physical applications). Ideally, a void found with this code is a local density minimum with an underdense region around it. A local density minimum can be found also in an overdense region of the box: therefore it is necessary to introduce some conditions in order to produce a suitable voids catalogue, which will be presented in the following sections.

Voids are joined together starting from density minima, following these steps:

1. The space is partitioned using the so called **Voronoi Tessellation**[3];

[1] ZOBOV can be modified in order to find voids in observational data too, ref. [32].

[2] A position file is a file that contains the position of all points (halos for what concerns this thesis work).

[3] It's a procedure by which the space is divided into cells. Voronoi Tessellation associates a cell to each particle i: the cell is defined as the region of space closer to the particle i than to any other particle. This way to *tesselate* the space leads to uneven void topologies and

2. To each cell ZOBOV associates a density which is, basically, the reciprocal of its volume;

3. The density minima are found: these are cells whose density is lower than the density of every other adjacent cells;

4. Around minima the algorithm identifies *zones*, i.e. the union of all the cells near a minimum, with a higher density than the one of the minimum's cell (of the zones);

5. Zones are joined together in voids with the *"water tank method*, which will be discussed in the section 3.1.1.

The physical significance criterion used in this thesis work is the one suggested by the author of the code (ref. [32]), and it consists of the use of the following density threshold in order to define underdense region as voids:

$$\rho_{min}/\rho_{mean} < 0.2\,, \tag{3.1}$$

where ρ_{min} is the density minimum of the void (whose numerical definition is going to be introduced soon) and ρ_{mean} is the mean density of the whole set of points.

Furthermore, ZOBOV measures the statistical significance for each void, by the parameter P_f, that quantifies the *fakeness probability* for each found under-density.

The quantity P_f is calculated as follows (see eq. 1 in ref. [32])

$$P_f(r) = \exp[-5.12(r-1) - 0.8(r-1)^{2.8}] \tag{3.2}$$

where r is the numerical density contrast which is calculated by the code as the ratio between the minimum density and the maximum density of each void (as explained in the list of section 3.1.2). The density contrast r is converted to a probability by a comparison to a Poisson particle distribution: eq. 3.2 is calculated by the fit of the cumulative probability function of the voids with a Poisson distribution of particles.

Thus, ZOBOV's spirit is to take all zones and voids found in the analyzed domain and then to exclude the one possibly arising within an over-dense region or simply generated by Poisson fluctuations in the distribution of points.

In section 3.3.1 we are going to discuss in details the choice which are made for both of these criteria (i.e. the statistical significance and the density threshold) for this thesis work.

shapes, and challenges the trivial spherical approximation.

3.1.1 From zones to voids: the *water tank* method

ZOBOV joins zones in voids following a non-trivial method which can be described with the analogy of filling with water a tank that has an irregular shape.

Picture a water tank with an irregular bottom surface. This irregular surface represents the analyzed density distribution, while the z-coordinate of a single point on the surface represents a single density value: the higher is z in the bottom of the tank the larger is ρ in the density distribution.

Let's now fancy that the tank which we have just described is about to be filled with water. For each zone i_{zone} (which, in the analogy we are presenting, is a basin in the irregular bottom surface of the tank), the water level is set to i_{zone}'s minimum density and then raised gradually: if the water level becomes higher than the edge of a zone, water may flows into adjacent zones, adding them to the void defined around the zone i_{zone}.

The process stops when water flows into a deeper zone (with a lower minimum than i_{zone}'s one), or if z is the deepest void when water floods the whole field. The final void associated to i_{zone} is defined as the set of zones contaning water just before this happens. The minimum density cell associated to a particle (which is defined as *core particle*) of the zone's i_{zone} is also the *core particle* of the void.

Many zones fail to annex surrounding zones: in this situation a zone has a void equal to itself.

This process, by joining many zones, can lead to very large voids. A choice on the significance level of voids and zones has to be made. This choice implies also exciding some zones which ZOBOV has joined together in the first place. We will discuss the criteria which will be used to define the edges of voids in the sections 3.3.

3.1.2 Outputs

The code produces three output files. The main ZOBOV output file, is a catalogue of voids, that includes this information:

- **Void Id**: identification number of the void;
- **Filevoid #**: the id number with which the voids are identified in the other two output files;
- **Core Particle**: the particle number of the void's (and zone's) *core particle* (i.e. if this number is 3, the *core particle* would be the third particle in the position files);
- **Core Density**: the density, in units of the mean, of the void's *core particle*;
- **Zone Volume**: the volume of the central zone of the void, in units of the volume occupied by a mean-density particle;

- **Zone#Part**: the number of particles in the central zone of the void;
- **Void#Zone**: the number of zones in the void;
- **Void Volume**: the volume of the void, in units of the volume occupied by a mean-density particle;
- **Void#Part**: the number of particles in the void;
- **VoidDensContrast**: the density contrast of the void, i.e. the ratio between the critical density at which water in that zone would flow into a deeper zone to the minimum density;
- **VoidProb**: the probability that DensContrast would arise from Poisson noise (using eq. 1 of the ZOBOV ref. [32]). This probability is based on a fit to the probability distribution of DensContrasts from a Poisson particle distribution.

The other two outputs contain information about which particles are in the zone i_{zone}, and which zones compose void i_{void}.

3.2 A test case

In order to understand how ZOBOV works and quickly verify whether its outcomes are robust, it is useful to test the algorithm with an input position file from a low-resolution simulation. We did this with a test file provided by the author of ZOBOV himself, Mark Neyrinck. This position file is the result of an N-body simulation with 64^3 particles (quite few, so that all the process should run rapidly). The positions of these particles are normalized to the box size, which can therefore be set as the user prefers. We used a box of $1Gpc$, which is equal to the box size of the CoDECS simulations.

This first approach is useful as long as it allows to take a look at ZOBOV's results without wasting much computational time.

3.2.1 Visual inspection of voids

After having run ZOBOV with the input file provided by Neyrinck and with the density threshold suggested by the same Neyrinck in ref. [32] (i.e., as already mentioned, $\rho_{min}/\rho_{mean} < 0.2$), its results are checked.

The method used is the one that follows. Once obtained the output from ZOBOV (which, as we have already pointed out, does not necessarily contain actual low density regions only) we select from it all the voids that have a fakeness probability lower than 1% and a *core particle* with density lower than $0.2 \cdot \rho_{mean}$. After such a selection procedure only 27 voids are left (without any cut there were ~ 100 of them).

By identifying the *core particle* of each void with a particle in the position file, it is possible to determine where the *core particle* of the void (i.e. the void density minimum, which at the moment is going to be considered the center of the void) is placed in the box. and, using a simple spherical approximation, we compute an effective radius, R_{eff}, starting from the Void Volume V_{void} in the ZOBOV output:

$$V_{void} = \frac{4}{3}\pi R_{eff}^3 \,. \tag{3.3}$$

The goal is to allow a direct visual inspection of the voids and of their associated radius under the spherical approximation. In fact, it one takes a look at particles and voids in a slice with a thickness of $1000 \times 1000 \times 100 Mpc$ centered at $z = 50 Mpc$ it is possible to directly check whether the obtained voids truly correspond to regions of space with a density of particle lower than the mean. Then, we move the center of the slice $100 Mpc$ higher in the z- coordinate, and we repeat this procedure ten times, so that one can visualize the whole box slice by slice.

The plots are shown in figures from 3.1 to 3.5.

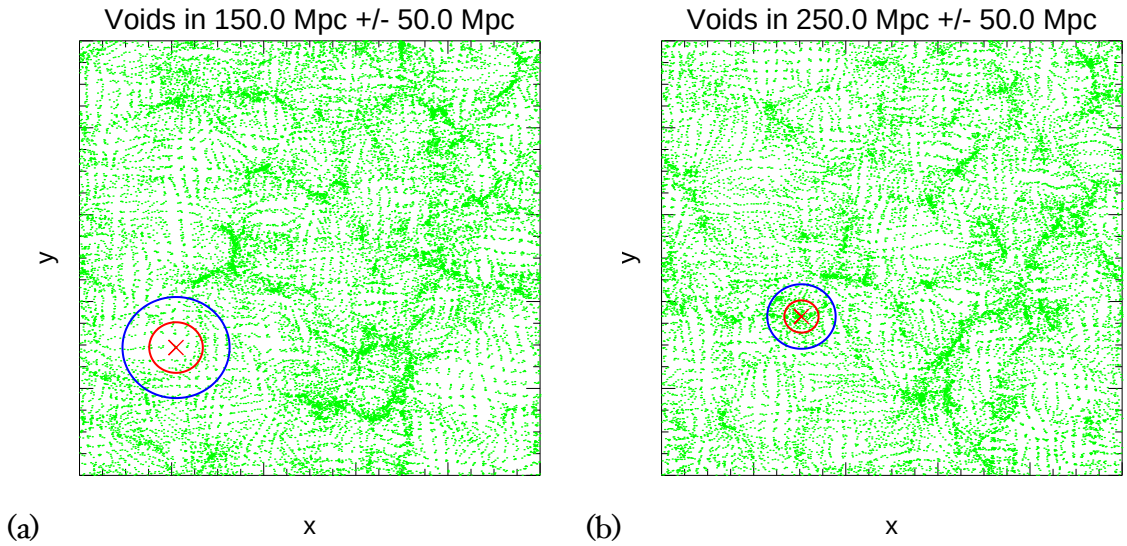

Figure 3.1: Slice centered at $z = 150 Mpc/h$ (a) and $z = 250 Mpc/h$ (b). The crosses show the position of the *core particles*, i.e the particles whose Voronoi cells are local density minimum. The blue circles have a radius equal to R_{eff}, while the red ones have a radius equal to $0.5 \cdot R_{eff}$

Looking at these plots it is possible to see that not always the core density particles seem to be located in a low density region. Sometimes, actually, the *core particle* appears to be on a filament (e.g. Fig. 3.1 (b), in some cases in Fig. 3.3 (a) e (b), and in Fig. 3.5). We did not report the slice centered at $z = 50 Mpc$ because there are no *core particles* in it.

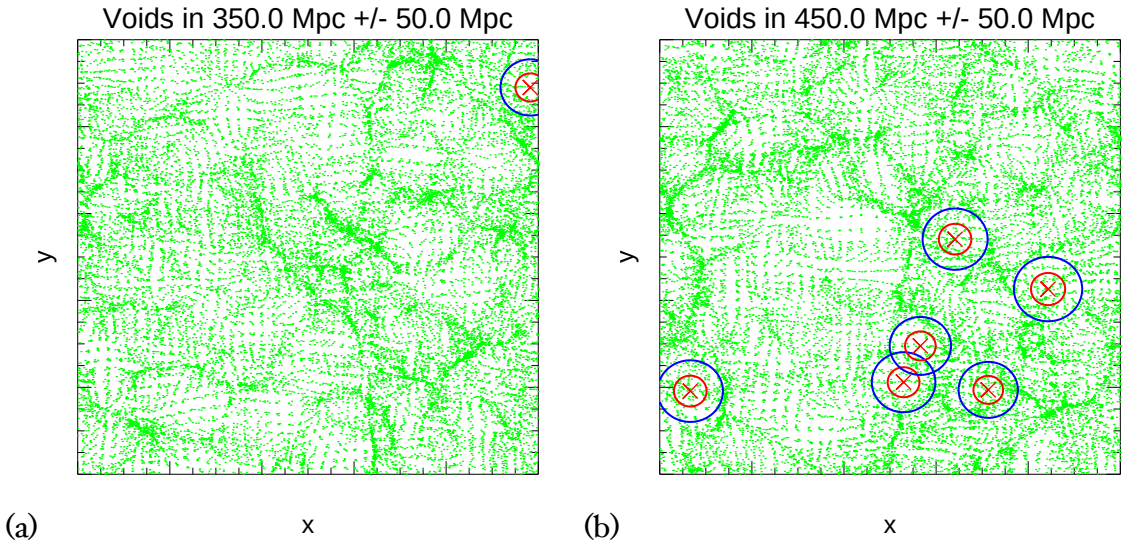

Figure 3.2: As figure 3.1 but for a slice centered at $z = 350Mpc/h$ (a) and $z = 450Mpc/h$ (b).

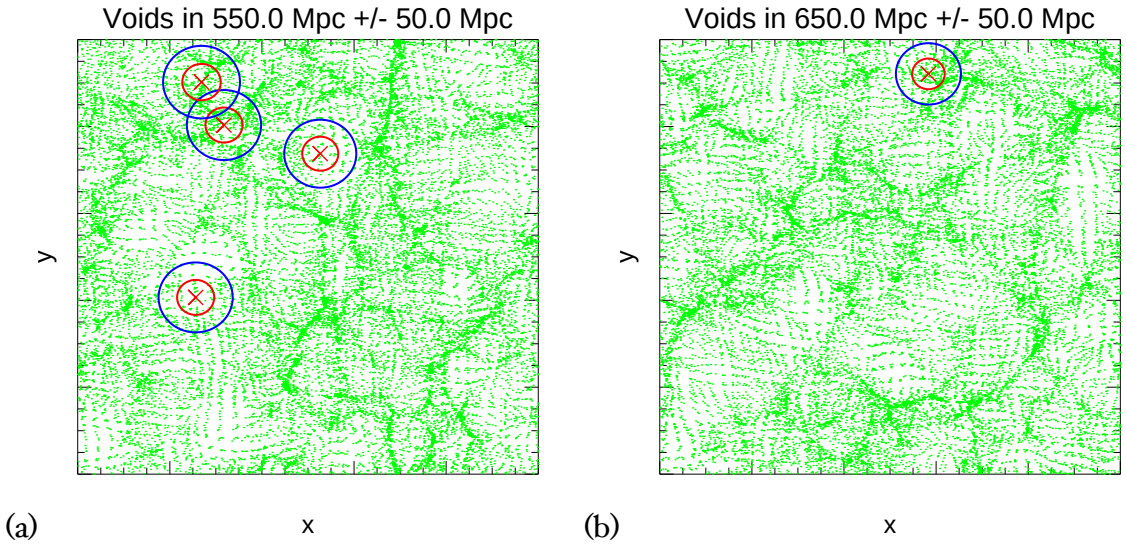

Figure 3.3: As figure 3.1 but for a slice centered at $z = 550Mpc/h$ (a) and $z = 650Mpc/h$ (b).

This last problem doesn't necessarily mean that ZOBOV doesn't work properly: the figures show $100Mpc/h$ portions of the box projected onto a 2D plane so it is possible that projection effects prevent a correct visualization. In fact if a filament is located just above or below a low density region, it would not be possible to discern one from another in a $x - y$ projection.

Thus, a more accurate visualization of the ambiguous voids has to be done. Let me consider a thinner slice of the box ($50Mpc/h$), and let me center it

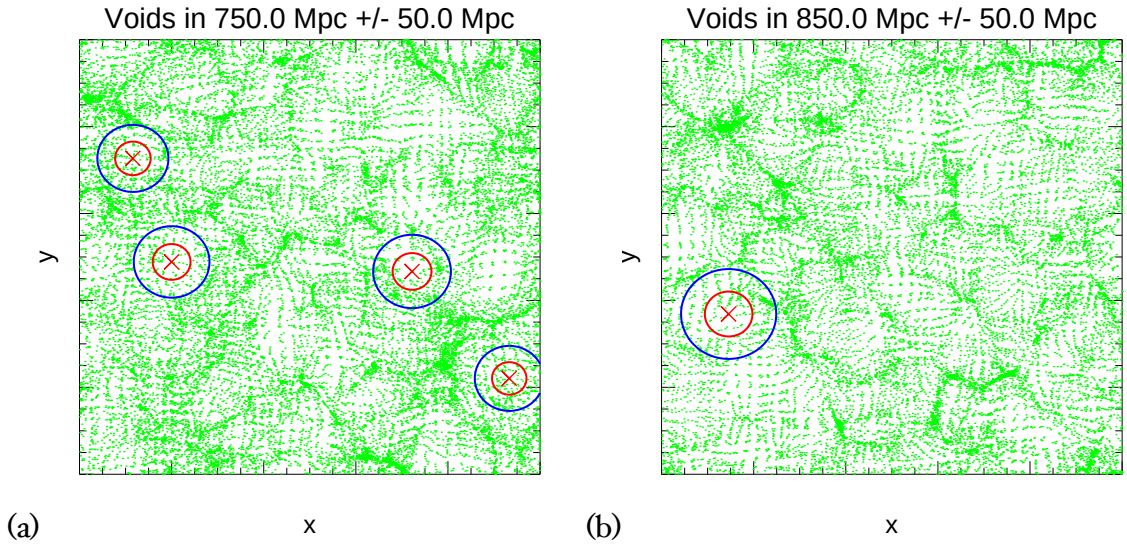

Figure 3.4: As figure 3.1 but for a slice centered at $z = 750Mpc/h$ (a) and $z = 850Mpc/h$ (b).

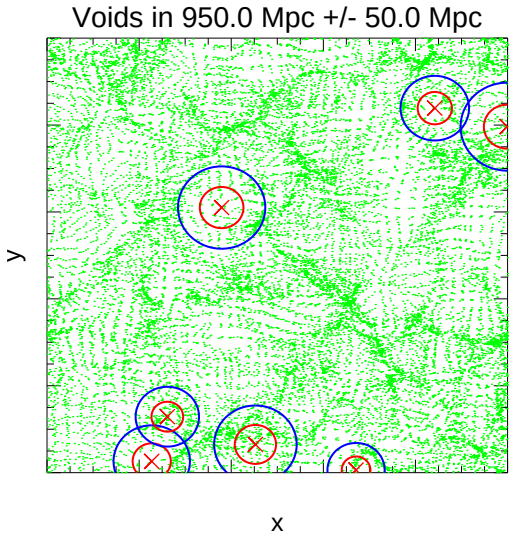

Figure 3.5: Slice centered at $z = 150Mpc/h$. The crosses show the position of the *core particle*s, i.e the particles whose Voronoi cells are local density minimum. The blue circles have a radius equal to one R_{eff}, while the red ones have a radius equal to $0.5 \cdot R_{eff}$

at the same z coordinate of the void's *core particle*. Furthermore, in order to avoid the possibility of having voids extending over one of the box boundaries, a change of coordinates is performed so that the *(x,y)* position of the

void's *core particle* looks at the center of the box[4] . In this way the neighbourhood of the *core particle* is clearly visible. With this new visualization, it seems much more neat that what ZOBOV found are density minima.

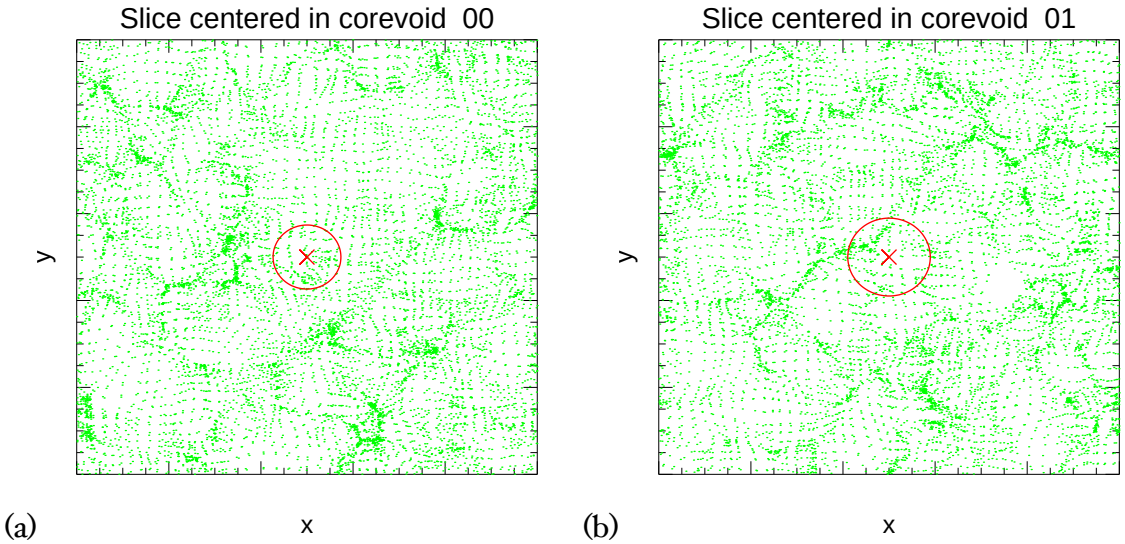

Figure 3.6: Slice centered at the coordinate z of the void #0 (a) and 1 (b), previously visualized in Fig. 3.5.

Another helpful test is to repeat these last plots for planes *(x,z)* and *(y,z)*.

[4]Numerical simulations of large scale Universe assume periodic boundary conditions. This means, for example, that the particle distribution in a little cube centered in $c = (x_c, y_c, z_c)$ inside the box, is equal to the particle distribution in $\hat{c} = (x_c + 1Gpc, y_c + 1Gpc, z_c + 1Gpc)$, if the box dimension is $1Gpc$. So, basically, the Universe created by these simulations is built by bricks (everyone equal to the Box) placed side by side in all of the three spatial dimensions.

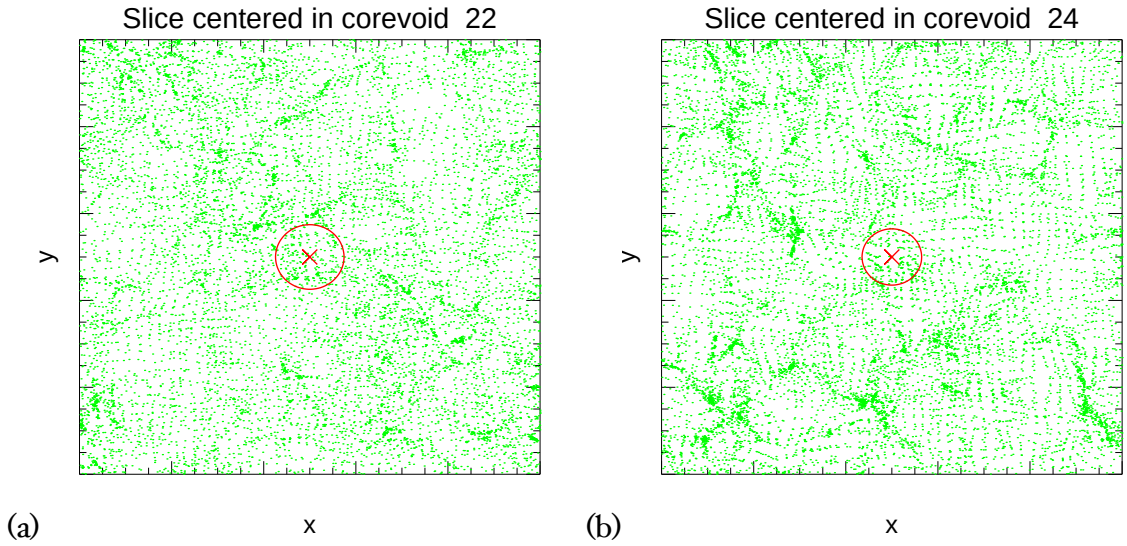

Figure 3.7: Slice centered at the coordinate z of the void #22 (a) and #24 (b), previously visualized in Fig. 3.3 (b) ed (a) respectively.

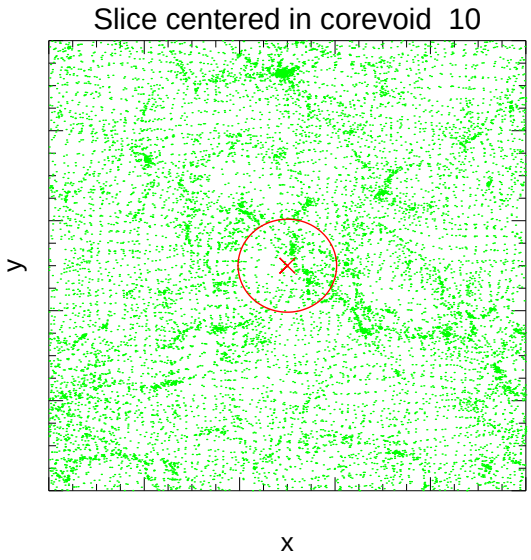

Figure 3.8: Slice centered at the coordinate z of the void #10, previously visualized in Fig. 3.1 (b).

The visual inspection gives us only few indications about the goodness of ZOBOV's output. Although the visualized *core particles* seem to be located in low density regions, it could be a subjective impression. Since figures show voids of any possible shape from a slice of the box, the visual inspection can not be exhaustive.

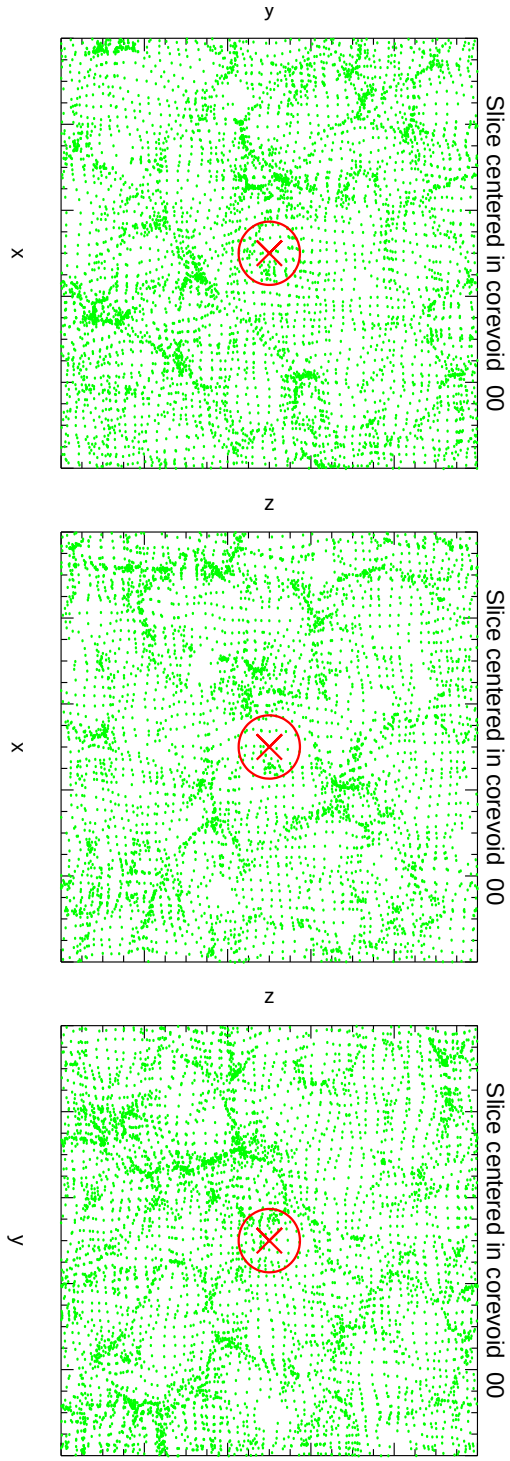

Figure 3.9: Slice centered at the coordinate x, y, and z of the void #0.

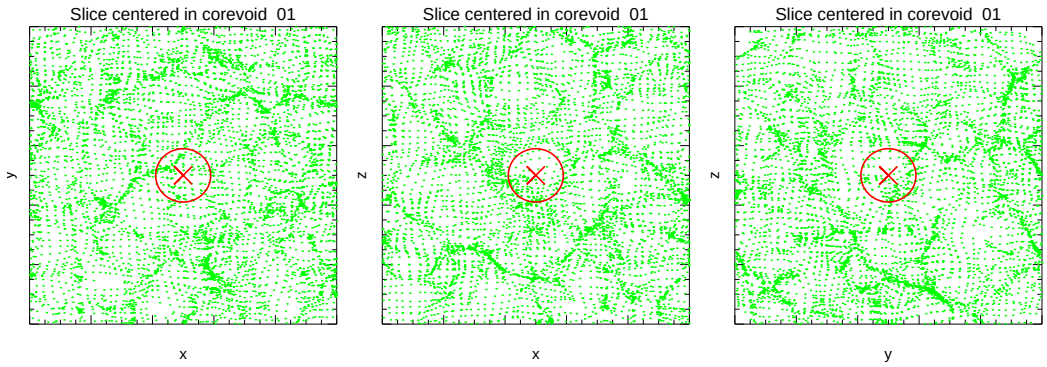

Figure 3.10: Slice centered at the coordinate x, y, and z of the void #1.

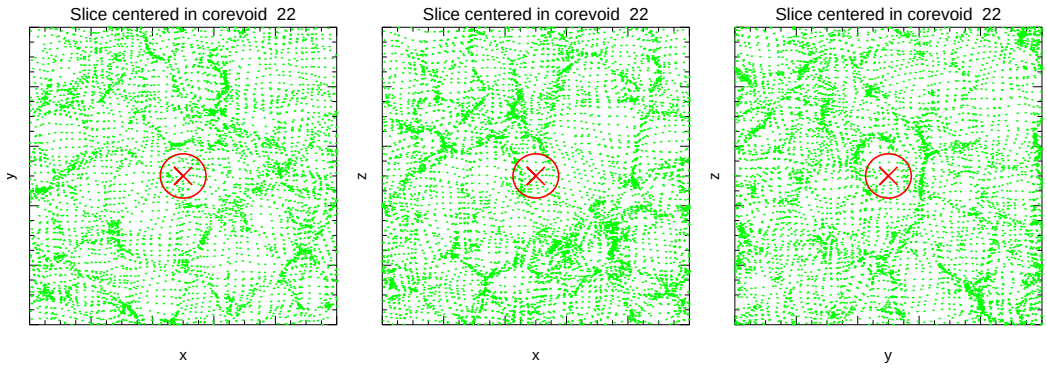

Figure 3.11: Slice centered at the coordinate x, y, and z of the void #22.

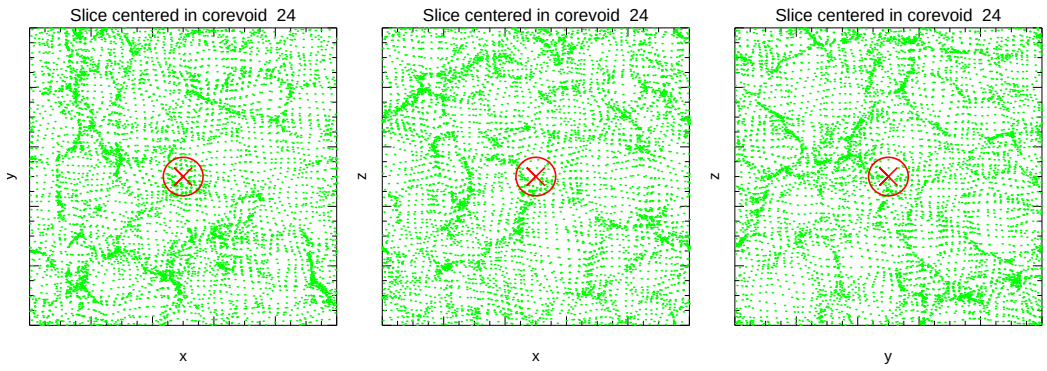

Figure 3.12: Slice centered at the coordinate x, y, and z of the void #24.

To still all doubts it is possible to take a look at the density profile of these objects. We proceed by considering voids as spheres centered in $\vec{x}_c$, the baricenter of the voids (while before the *core particle* was considered the center), calculated as follows:

$$\vec{x}_c = \frac{1}{V_{void}} \sum_{i=1}^{N_v} \vec{x}_i^{halo} \cdot V_i^{halo} \,, \tag{3.4}$$

where $\vec{x}_i^{halo}$ and V_i^{halo} are the position and the volume of the i-halo respectively, and V_{void} is the volume of the void. The radius of the spheare, R_{eff}, is obtained from the volume provided by ZOBOV using eq. 3.3:

$$V_{void} = \frac{4}{3}\pi R_{eff}^3 \,.$$

An exemplifying density profile is presented in fig. 3.13 and it can be compared with a density profile found in the literature, fig. 1.2. The two profile are quite similar: they both show an evident under-density at low radii, R. While the profile in fig. 1.2 also presents the expected slight over-density at $R \sim R_{eff}$ (see 1.3) as it is expected by predictions (see ref. [52]) this feature is not showed by the void in fig. 3.13. At this level, this is not a major issue: in fact, it is important to remember that a very low resolution N-body simulation is analyzed in this test case, while the density profile in fig. 1.2 is computed in a high-resolution simulation and it is expected to show a better agreement with prediction and observation than the one which is shown by fig.3.13.

At this level of sophistication, it is important to note that in fig. 3.13 at small radii (lower than R_{eff}) the density is lower than the mean density. It is now possible to appreciate with a good confidence that ZOBOV really finds low density regions of the Box.

3.3 Building the catalogue

After having tested ZOBOV in general, We want now to develop suitable criteria to create our catalogues. In order to do this we start defining the method by running the algorithm on the halo catalogue at $z = 0$ of the CoDECS simulation run in the context of the standard ΛCDM model (ΛCDM-CoDECS). We will later use the same *pipeline* to create the catalogues for all models at various redshifts.

3.3.1 Our criteria

In our present approximation the voids are spheres, with a radius, R_{eff}, given from eq. 3.3 and centered in the baricenter of the void calculated from eq.3.4. This kind of approximation has already been taken in consideration in the literature (e.g. ref. [53]).

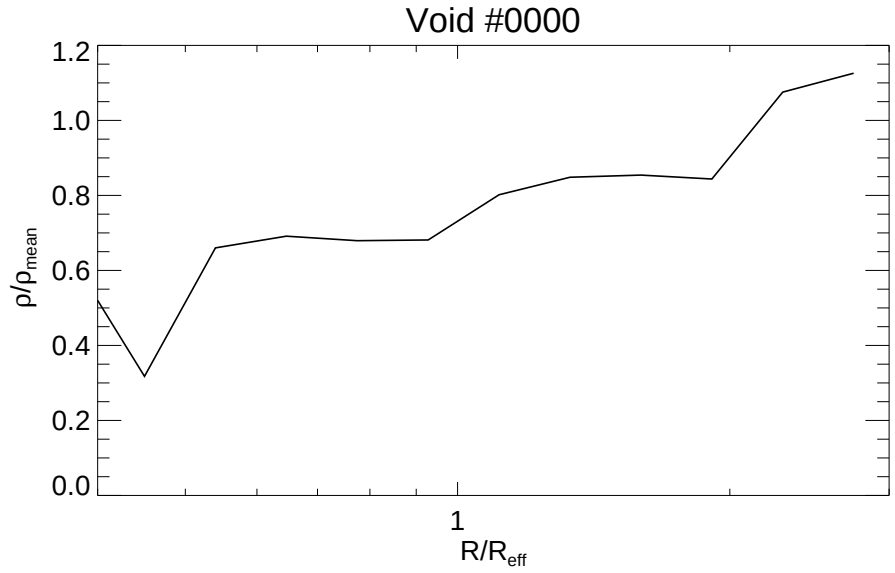

Figure 3.13: Density profile of void #0 found in Neyrinck test file. The low definition of the simulation is not helpful in showing a smooth density profile, but the shape shows the aspected underdensity region at small radii.

Statistical and physical conditions

As explained in section 3.1, this code finds any zone around a local minimum in the density distributions and report it as a void. Thus, it is necessary to manipulate the catalogue which ZOBOV creates so that:

1. All the zones considered are actually low density regions (because, as we have already pointed out, also in high density regions of the box there are depressions in the density distribution, but these may have density greater than the mean density, so they are not voids);

2. They are not just a statistical fluctuation in the density distribution.

To avoid the first problem we constrain all the voids in our catalogue to have a *core particle* with density, ρ_{min}, such that $\rho_{min}/\rho_{mean} < 0.2$ (*physical condition*), as it is suggested by the author of the code. Furthermore, in order to take care of the point 2, we need to select a level of significance We consider appropriate (*statistical condition*).

It is possible to repeat the test run by Mark Neyrinck in section 2.4 of ref. [32]. The results are reported in table 3.1. To repeat this test we apply 4 cuts on ZOBOV outputs so that in each cut we consider a different level of significance[5].

[5]Level of significance (σ), density ratio, and fakeness probability as defined in ref. [32] are correlated so that, once one of these variables is fixed, the other two are univocally determined.

σ	$P_f(r)$	r	Voids	Voids ($\rho_{min} < 0.2 \cdot \rho_{mean}$)
0	1	1	10211	4836
1	0.317	1.22	4724	3225
2	4.55×10^{-2}	1.57	1667	1530
2.7	1×10^{-2}	1.91	912	882
3	2.70×10^{-3}	2.00	593	585

Table 3.1: Void abundances for various P_f in ΛCDM of CoDECS halos at $z = 0$. The first column reports the significance level σ, while the second and the third list the fake probability $P_f(r)$ and the density ratios r (which are both known from the ZOBOV output, so these are the critical values we require in order to fulfill a certain significance level). The fourth column shows the number of voids under the corresponding σ and the fifth adds the constraint that $\rho_{min} < 0.2 \cdot \rho_{mean}$.

Let's compare the density contrast distribution of these different samples of voids. The density contrast, $\delta\rho$, is given by eq. 3.5:

$$\delta\rho = \frac{\rho_{void} - \rho_{mean}}{\rho_{mean}}. \tag{3.5}$$

where the density of the void, ρ_{void}, is computed considering the density of the sphere centered in $\vec{x}_c$ with $R = 1/4 \cdot R_{eff}$.

In fig. 3.14 the distributions of the density contrast of different void samples are reported. The samples are extracted from the ZOBOV's catalogues following the criteria we have just explained and that are summarized in Table 3.1.

Our *physical condition* is going to be the one suggested in ref. [32], $\rho_{min} < 0.2 \cdot \rho_{mean}$. Since the major goal of this thesis work is studying the statistical properties of voids, as *statistical condition* the 2σ significance is kept. With this choice a large number of voids in the sample are still present (see Table 3.1, 5^{th} column) without having a protruding tail in the density contrast distribution (fig. 3.14).

Edges

We have already mentioned that zones, which basically are low density regions themselves, can be joined together in voids as explained in section 3.1.1. Since we have decided to remove all voids that do not fulfill our *statistical condition*, we now need to excise from the *parent void* all the *subvoids* (i.e zones annexed to a void, see section 3.1.1) that are exceeding the requested significance level.

If a *subvoid* (i.e. a zone which ZOBOV annexed to another) is removed from a *parent void* (i.e. the zone to which the subvoid was annexed) then **all the subvoids which join the parent void in the same flooding event**

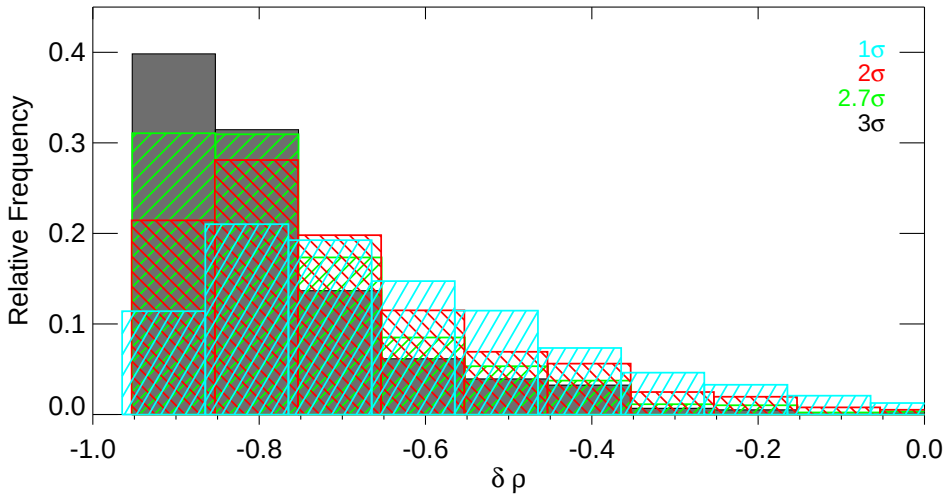

Figure 3.14: Distributions of density contrast for ΛCDM - CoDECS of halos at $z = 0$ for different sample extracted from ZOBOV catalogue following the cut's criteria shown in Table 3.1. It is possible to appreciate that the 3σ distribution is the steepest one (dark grey), with the highest peak and the shortest tail, while in other distributions [2.7σ (green), 2 (red) and 1σ (light blue) respectively] the peaks become lower and lower and the tails increase to positive values of $\delta\rho$.

as that subvoid (once again, we are using the water tank analogy as it is described in section 3.1.1) **and in subsequent ones need to be also removed**, see section 2.5.1 of ref. [32].

This last assumption imposes that all of the zones which compose a final void (after the exclusion of some of the zones joined by ZOBOV) must be adjacent. This choice has to be made in order to avoid the possibility to consider voids with disjoined pieces which spread across the box. In fact, if the above mentioned criteria is not applied to the sample, this will necessarily include in the catalogue some voids with disjoined parts, which are not of interest for this thesis work.

All the criteria which are presented in this section are going to be used to define voids catalogues in the CoDECS simulations. These are the largest cosmological N-body simulations of coupled DE cosmologies to-date, as presented in the last chapter. Using the *pipeline* we have developed with the test case described in this section, we create a void catalogue for all the cosmological models included in the CoDECS suite at different redshifts. In the next chapter we are going to present the statistical analisys of void catalogues of the CoDECS simulations.

Chapter 4

Statistical Properties of Voids

As pointed out in chapter 1, the last decade has witnessed the establishment of a Standard Cosmological Model, based on homogeneous and isotropic solutions of Einstein's equations of General Relativity 1.5 (described by the Friedmann-Lamaitre-Robertson-Walker metric eq. 1.12), upon which small initial perturbations are generated. These primordial fluctuations grow by gravitational instability to form the galaxies and the large-scale structure we observe around us today (ref. [3]). In order to match the theoretical predictions of this model with cosmological observations that show an accelerated expansion of the Universe (ref. [20], [21]) the model requires the addition of a Dark Energy component, whose simplest form is a Cosmological Constant, Λ.

Although this model has been remarkably successful in accounting for almost all available observational data, it leaves many questions unanswered. In chapter 2 the major problems by which ΛCDM is affected are reported and the scalar field scenario, which is making a great effort to solve them, is also introduced.

A further possibility to compare ΛCDM results with Quintessence and cDE outcomes can be provided by the comparison of the statistical properties of cosmic voids (the general properties of which are presented in section 1.3) in different cosmological scenarios. In chapter 3 it is presented the method by which a voids catalogue can be defined with this purpose, while, in this chapter, we will discuss our statistical analysis of voids properties.

By means of the pipeline which was developed following the criteria described in section 3.3, a voids catalogue is created for all of the models (which are described in section 2.2) included in CoDECS, the largest suite of publicly available cosmological and hydrodynamical N-body simulations to date featuring a direct interaction between DE and CDM (see section 2.3). The tracers of the matter density are going to be the halos, since the halo catalogs of the CoDECS simulations are considered as input of the void finder.

In this chapter we are going to present the statistical properties of cosmic

voids in different cosmological scenarios.

Our analysis is run on each model considering 5 different redshifts ($z = 0$, 0.26, 0.55, 0.82, 1.0) in order to analyze also the possible differences at different evolutionary stages. It is not always relevant to show all of the results at all of the redshifts: in many cases we will show at first the outcomes at $z = 0$, 0.55, 1.0, and eventually present the results at $z = 0.26$ and $z = 0.82$ if they show relevant features.

4.1 Voids volume fraction evolution

One of the first comparisons that it is possible to perform thanks to our pipeline which was developed starting from ZOBOV, concerns the evolution of the volume occupied by voids at different cosmic times. Fig. 4.1 shows such a feature, considering the evolution with respect to the redshift of the volume fraction of voids

$$\frac{V_{voids}}{V_{tot}}\,, \tag{4.1}$$

where V_{voids} is the sum of all voids volume in a fixed snapshot of the simulation and V_{tot} is the total volume of the Box, which is always $(1\,Gpc/h)^3$. In order to assign an error to this result we divide the Box in 8 sub-cubes with a side $l = Box/2$, and we calculate the volume fraction of the voids in each of these cubes V^i_{voids} in the ΛCDM model. The difference between the volume fraction of voids in the Box and the mean voids volume fraction (calculated among these 8 cubes) provides a dispersion value d_v computed as follows:

$$d_v = \frac{V_{voids}}{V_{tot}} - \frac{1}{8}\sum_i^8 \frac{V^i_{voids}}{(Box/2)^3}\,. \tag{4.2}$$

Thanks to d_v we can compare all of the models we are considering with ΛCDM model.

No significative difference in the evolution of voids volume fraction among the considered models is shown by this figure: in fact the voids volume evolution of all of the models is included in the dispersion area (grey). As expected, the volume fraction of voids generally increases with the decreasing of the redshift. In fact due to gravitational instability voids grow with respect to the time. An exception is added by EXP003: a slight regress of the V_{voids} can be appreciated from $z = 0.26$ to $z = 0$. We can argue whether or not this is a significant feature: on one hand EXP003 is the model that presents the strongest coupling among CoDECS simulations (as pointed out in table 2.2) and this property provides the strongest differences in the evolution of the perturbations with respect to the ΛCDM scenario (see eq. 2.23) so we are expecting to find some differences between these two models. Nevertheless, the values of the volume fraction of EXP003 at $z = 0$ and $z = 0.26$ are very

similar and they can be considered equal within an error of 0.2%, so probably the comparison of the evolution of the volume fraction of voids does not represents a good test to stress these differences.

The figure also shows that the ΛCDM model has generally the lowest volume fraction (except for $z = 0.26$) with respect to all the cosmologies under investigation.

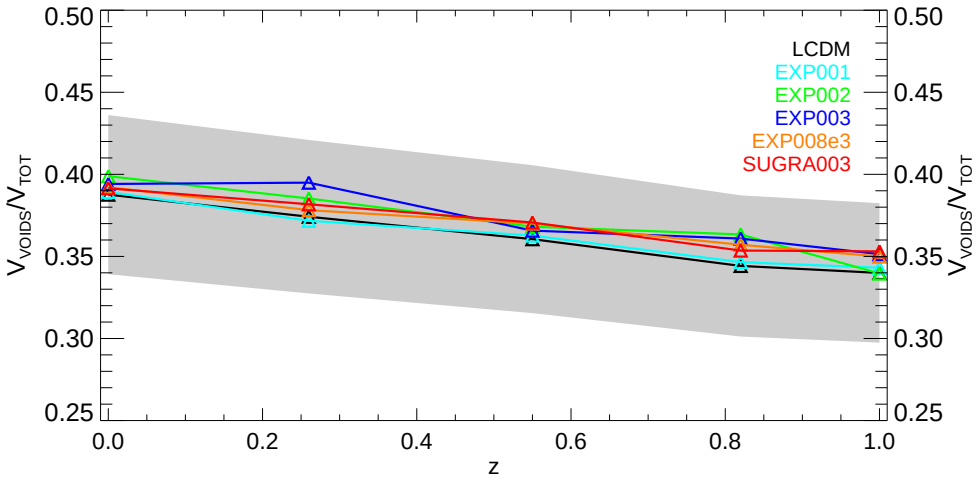

Figure 4.1: Evolution of the volume fraction of voids in the halo catalogs of the CoDECS halos simulations with respect to the redshift. The slope of the different curves is very similar, even though the EXP003 model (blue) shows the unusual feature to possess a smaller voids volume fraction at $z = 0$ than at $z = 0.26$. With the exception of the point at $z = 0.26$, the Standard ΛCDM model (black) has always the lowest voids volume fraction with respect to all models in the CoDECS suite. The dispersion area (grey) is calculated as described in this section.

4.2 Rarest objects: the largest void

It is possible to compare the evolution with redshift of the largest voids included in the catalogues of the different models. We consider the 8 biggest voids included in our catalogues at fixed model and at fixed redshift and we calculate the mean radius among these 8 objects R_{max}^{mean} for all of the redshifts.

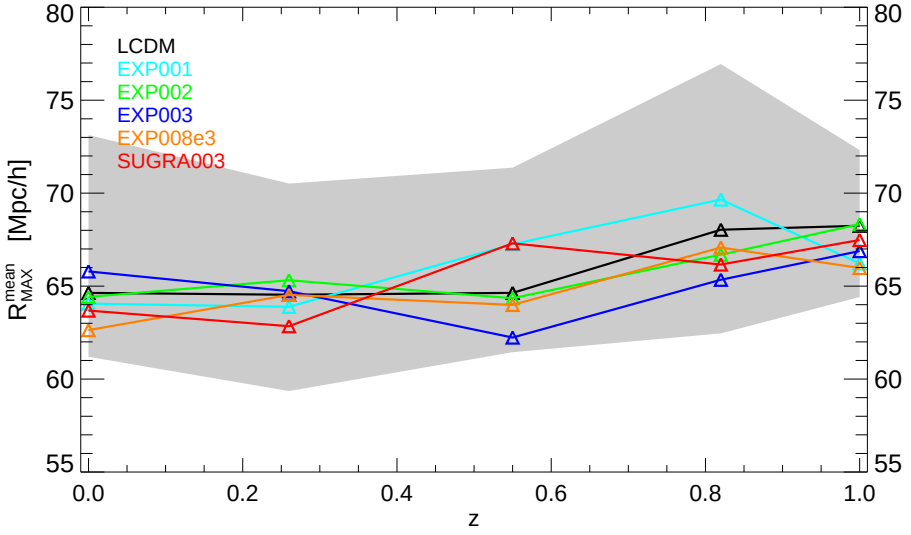

Figure 4.2: Evolution of the maximum value of R_{eff}, i.e. R_{eff}^{max}. The plot does not show a clear trend, but it is possible to appreciate that the model EXP003 (blue) is quite always the model with the smallest R_{max}^{mean} at $z > 0.5$.

The comparison is reported in fig. 4.2 and it shows no evidence of a clear trend in the evolution of the largest voids in the considered samples. The grey area shows the region in which the largest 8 voids of ΛCDM spread (i.e. the top limit of the grey area is drawn by the largest voids in ΛCDM while the bottom limit is fixed by the evolution of the 8^{th} largests voids of ΛCDM). Nevertheless we can see that model EXP003 generally shows a small R_{eff}^{max} for redshifts z greater than 0.5. This last statement is consistent with the results of the comparisons that will be presented in the following discussions: new evidence reported in section 4.4 will confirm that the EXP003 model shows an excess of voids with small radii with respect to the ΛCDM model. Thanks to these two outcomes it is possible to conclude that in the EXP003 catalogue are generally included the smallest voids among the considered cosmologies at $0.5 < z \leq 1.0$.

The biggest void in all of our catalogues is included in the catalogue of EXP003, and has a $R_{eff} \sim 79 Mpc/h$.

4.3 Two-point correlations function

As pointed out at the beginning of section 1.3 the Cosmological Principle (which was introduced in section 1.1.1) is not perfectly realized in nature at all the scales: on sufficiently small scales the Universe is not homogeneous and isotropic, structures form and arrange themselves like a "net", the so called the cosmic web. In fact, galaxies generally are found to be arranged in clusters of galaxies and filaments connecting the clusters. It is possible to argue whether or not voids also have the property to cluster, i.e. if they are not arranged in a homogeneous distribution across the Universe.

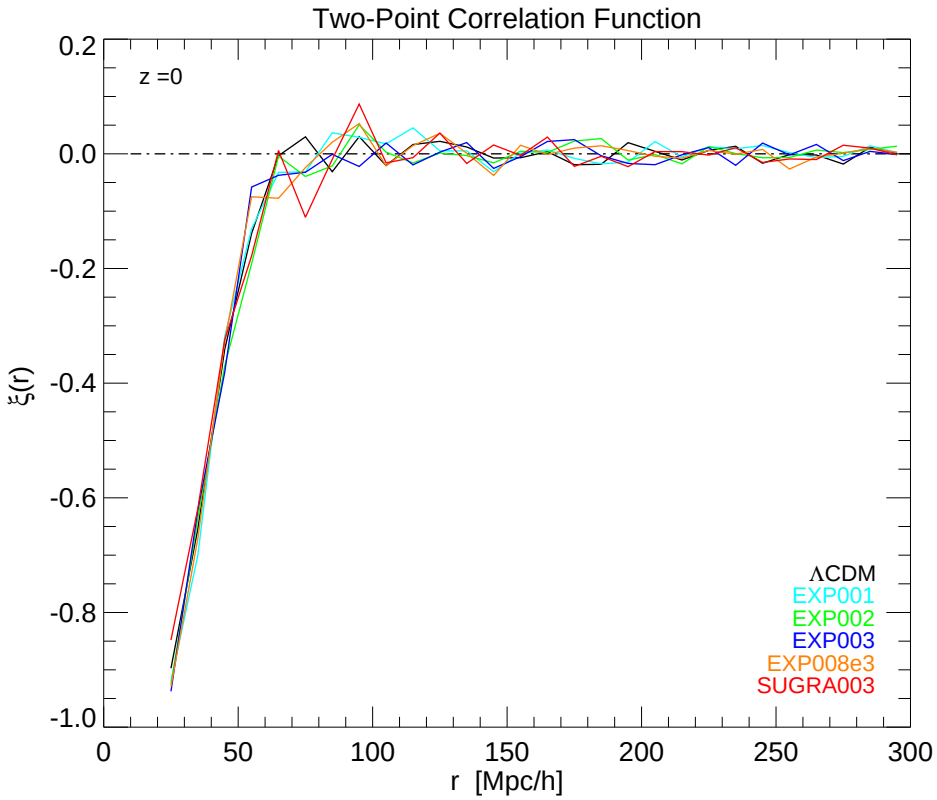

Figure 4.3: Two-Point Correlation Function for voids, calculated using eq. 4.4, for all the models included in the CoDECS suite at $z = 0$. In the range $20Mpc/h \lesssim r \lesssim 100Mpc/h$ an anti-correlation is present, due to the fact that the scales are similar to the dimensions of the voids (as we will see in next section, see e. g. fig. 4.12). At radii bigger than $\sim 100Mpc/h$ no signal is shown, the TPCF oscillates around zero.

If the distribution of the matter in the Universe is considered as a set of points (in this case voids) and n is the mean density of points per unit volume, the probability to find a point in the infinitesimal volume dV is

$$dP = ndV \, . \tag{4.3}$$

The *Two-Point Correlation Function* $\xi(r)$ of this distribution is defined by the joint probability to find two points separated by a distance r:

$$d^2P = n^2 dV_1 dV_2 [1 + \xi(r)] \,, \tag{4.4}$$

where dV_1 e dV_2 are both infinitesimal volumes, as the excess probability with respect to a homogeneous distribution. Under the assumption of isotropy, $\xi(r)$ has a dependency by r only (see ref. [26]).

Since the positions of the centers of the voids are known in our catalogues, the Two-Point Correlation Function (TPCF) $\xi(r)$ can be calculated for our voids by means of an algorithm developed at the University of Bologna (kindly provided by F. Marulli). This algorithm generates a catalogue of objects with a random distribution (in the same range of positions of the catalogue of voids under analysis) and counts the number of pairs of voids (VV), the number of pairs of random points (RR) and the number of pairs constitued by one void and one random (VR) in the samples. The TPCF $\xi(r)$ can be finally calculated using the standard Landy & Szalay estimator (see [16]):

$$\xi(r) = \frac{VV(r) - 2VR(r) + RR(r)}{RR(r)} \,, \tag{4.5}$$

where $VV(r)$, $VR(r)$ and $RR(r)$ are the fraction of void-void, void-random and random-random pairs found in the sample respectively, with spatial separation in the range $[r - dr, r + dr]$. The value of dr is fixed at $5Mpc/h$ (since the bin size is chosen to be $10Mpc/h$).

The results of the calculation of the TPCF are reported in figs. from 4.3 to 4.5. The TPCFs of all of the models included in the CoDECS suite show the same qualitative trend, i.e. an anti-correlation at small distances (in the range of $20Mpc/h \lesssim r \lesssim 100Mpc/h$), and a zero value at radii greater than $\sim 100Mpc/h$. The evolution with the redshift does not seem to affect the TPCF.

Since the value of the TPCF oscillates around zero for all of the models and for all the redshifts at scales greater than the typical scale of a void, it is therefore possible to conclude that *voids do not form bigger super-structures such as "void clusters"* for all of the models we have analyzed at $z \leq 1.0$. The distribution in the Universe of the voids included in these catalogues is almost homogeneous at scales greater than $\sim 80 - 100\, Mpc/h$, in perfect agreement with the Cosmological Principle.

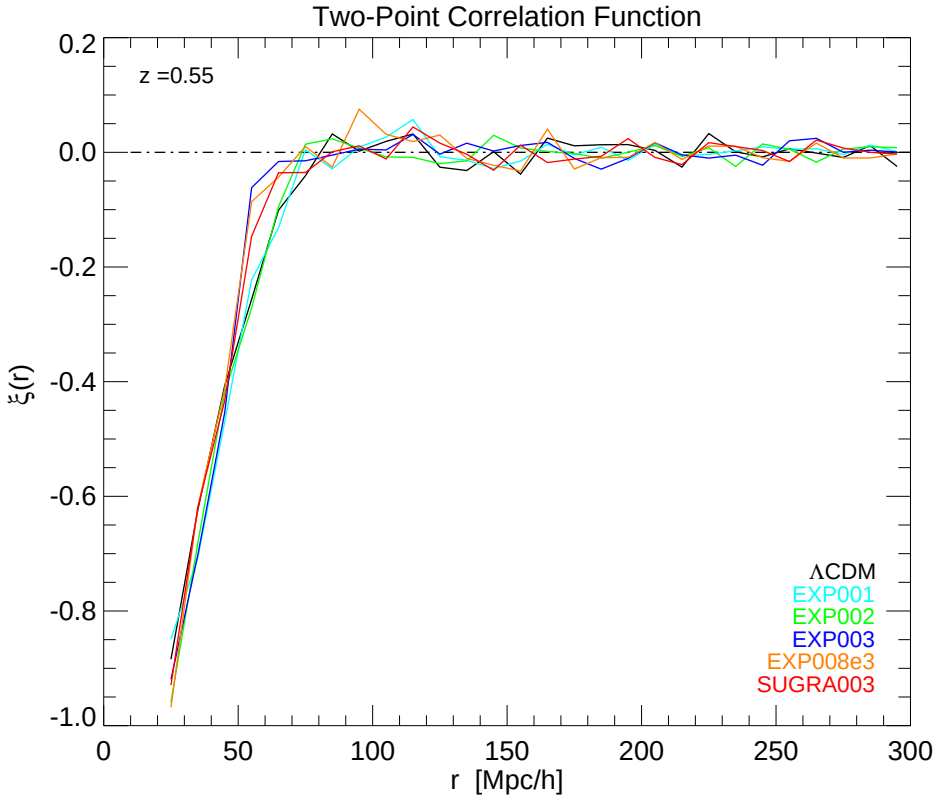

Figure 4.4: Same as fig. 4.3 but at $z = 0.55$

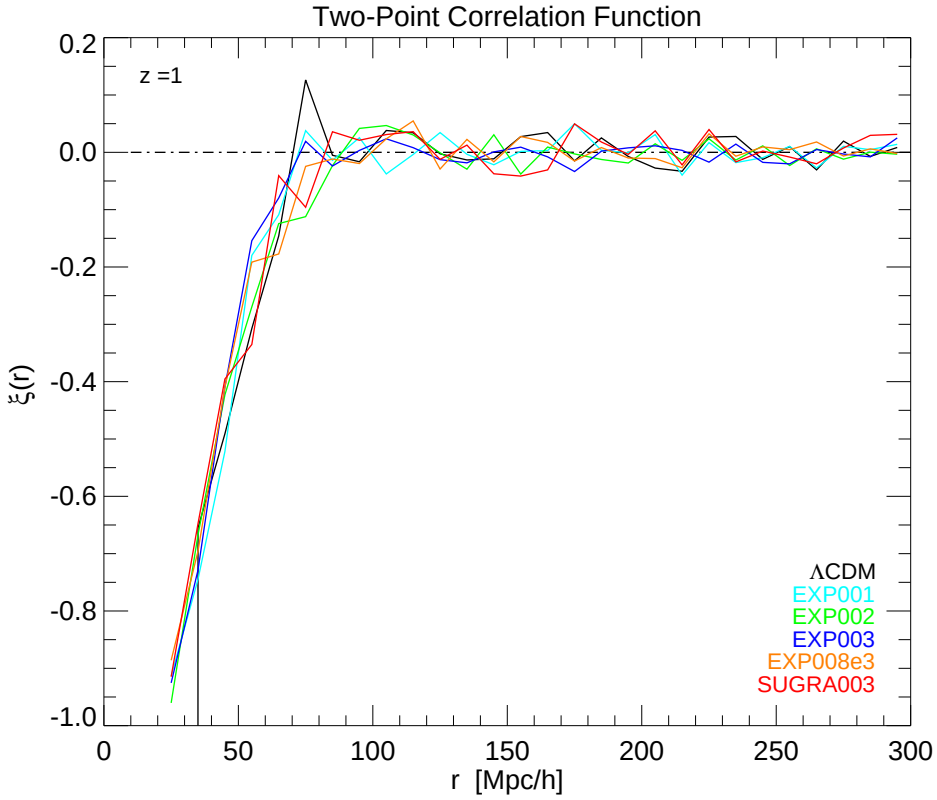

Figure 4.5: Same as fig. 4.3 but at $z = 1.0$

4.4 Size distribution functions

Another possible strategy to point out the differences between properties of voids which belong to different cosmological scenarios, is provided by the comparison of their respective *Size Distributions*. We recall that we defined voids as spheres which are centered in the baricenter of the void and whose radius is calculated starting from *Zobov*'s voids volume as it is stated by eq. 3.3. To each void a radius is associated, so it is possible to compute the distribution function of voids radii (i.e. the *Size Distribution Function*) or, equivalently, the distribution function of voids volumes (i.e. the Volume Distribution Functions). We decided to compute the Size Distribution function that shows how many voids with a fixed radius are found in the catalogues.

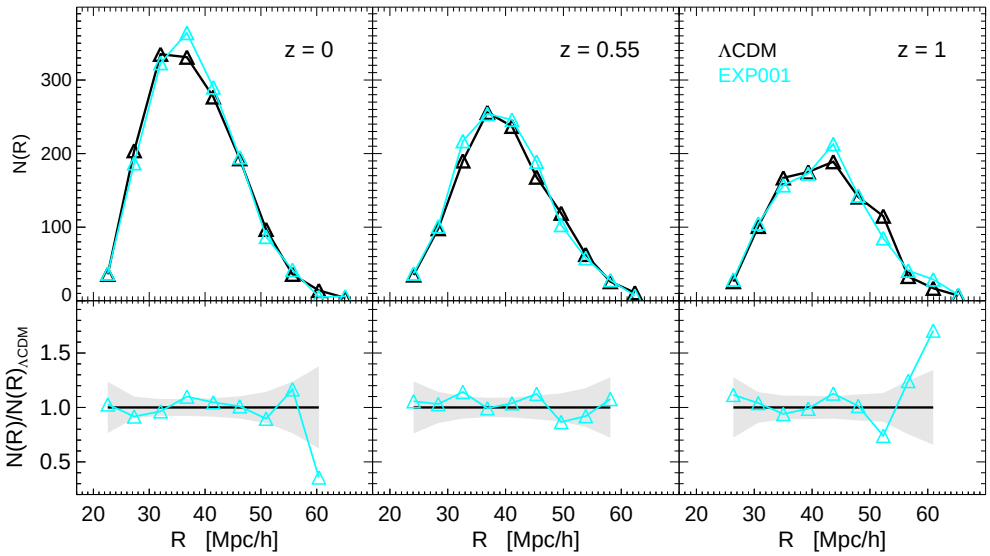

Figure 4.6: Differential Size Distribution Function for the model EXP001 of CoDECS simulations (cyan) compared with the Differential Size Distribution Function of ΛCDM (black) at different redshifts. In order to stress the differences among the two models, the ratio to the ΛCDM distribution is also plotted in the bottom panels. The grey area represents the statistical error calculated as the error of a Poisson Distribution.

We will present two possible methods to calculate the Size Distribution Function of voids in our catalogues: the *Differential Size Distribution Function* and the *Cumulative Size Distribution Function*. The former shows how many voids have a radius in a fixed range of radii, while the latter displays the number of voids with a radius R_{eff} greater than a fixed radius r.

Let us introduce the results produced by means of the Differential Size Distribution Function. In order to calculate it, it is necessary to introduce a bin, the dimension of which is calculated as follows: at fixed redshift we select

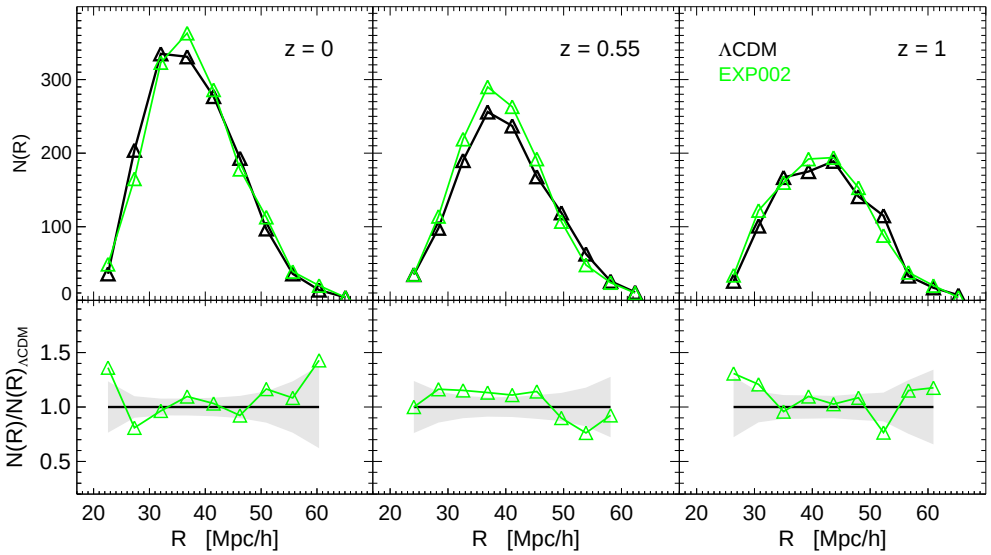

Figure 4.7: Same as fig. 4.6 but for the CoDECS simulations of EXP002 (green).

the maximum radius between the minimum radii of all models, r_{min}, and the minimum radius among the maximum radii of all models, r_{max}. Thereafter the dimension of bins d_{bin}, is defined as:

$$d_{bin} = \frac{r_{max} - r_{min}}{N}, \tag{4.6}$$

where N is the number of bins that is chosen to be 10. Finally, the Differential Size Distribution Function is calculated by counting the number of voids having a radius included in the range of each bin. In figs. from 4.6 to 4.11 the Differential Size Distributions of the voids of our different catalogues are shown. To stress the differences between the models the ratio between that of all models and Differential Size Distribution of ΛCDM is calculated and shown in the bottom panels of all of the figures. The grey area represents the statistical error calculated as the error of a Distribution of Poisson.

The small deviations of model EXP001 (see fig. 4.6) from ΛCDM are all included in the statistical error, at all the considered redshift.

While model EXP002 (see fig. 4.7) shows a slightly larger number of voids having a small radius than ΛCDM at $z = 0.55$, the most relevant differences are shown by model EXP003, which is the model that possesses the strongest value of the coupling function among the considered models. In fact, it is possible to appreciate that model EXP003, at redshift z greater than 0.5, presents an excess of voids with small radii with respect to the standard model. This feature is confirmed by fig. 4.9, in which it is also reported the Differential Size Distribution Function calculated at $z = 0.26$ and $z = 0.82$. For redshift $z = 0.82$ the excess of voids with small radii is also shown.

The Differential Size Distribution functions of models EXP008e3 and SUGRA003 (see figs. 4.10 and 4.11 respectively) slightly deviate from the distributions of ΛCDM model.

We observe that all of the discrepancy that the cDE models included in our discussion present with respect to the Standard Model are generally shown at $z = 0.5$ and $z = 1.0$

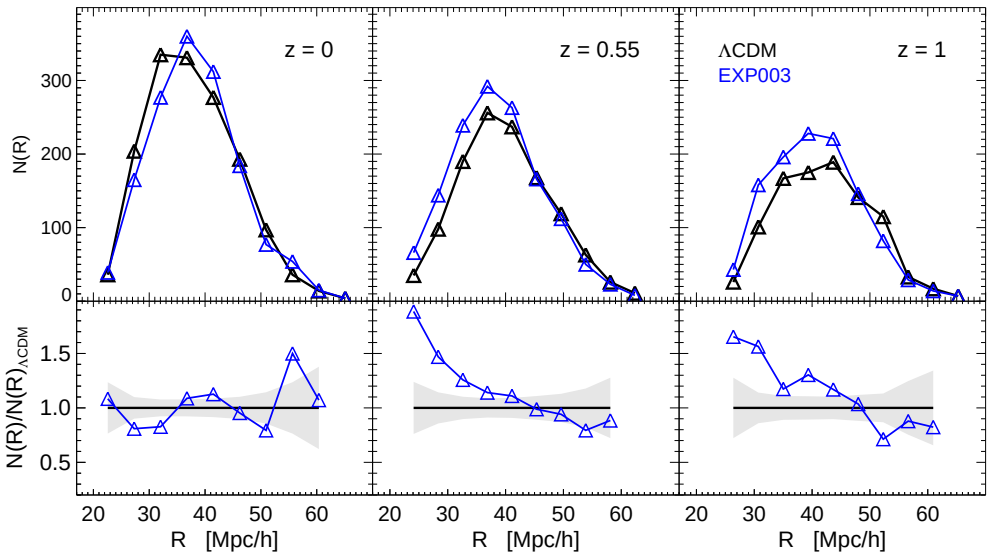

Figure 4.8: Same as fig. 4.6 but for the CoDECS simulations of EXP003 (blue).

As we have mentioned before, there are two possibilities to compute the Size Distribution Function, the second of which is represented by the so called Cumulative Size Distribution Function. It consists in counting the number of voids which possess an effective radius R_{eff} larger than a given radius R. In fig. 4.12 it is reported the Cumulative Size Distribution Function of all models a $z = 0$, 0.55, $z = 1$, and the ratio to the ΛCDM distribution.

Looking at Fig. 4.12 it is possible to observe that at large radii (i.e at radii $R > 60Mpc/h$) the ratio between the distributions of different models is still very noisy. The 8 biggest voids of each catalogue were removed in order to obtain smooth ratios but the noise persists. We have to consider that only few voids have a R_{eff} greater than $60Mpc/h$: so it is not surprising that the noise persists at large radii, and the results at those radii should be carefully considered. Anyway, the models with the strongest coupling (EXP002 and EXP003) show a larger fraction of big voids than the Standard Model at $z = 0$, while at $z = 1.0$ the model EXP001 shows a remarkably larger number of voids with $R > 50Mpc/h$ than ΛCDM.

Looking at the bottom panels (in particular, in fig. 4.12) confirms what we have observed so far at small radii: while at $z = 0$ the Cumulative Distribu-

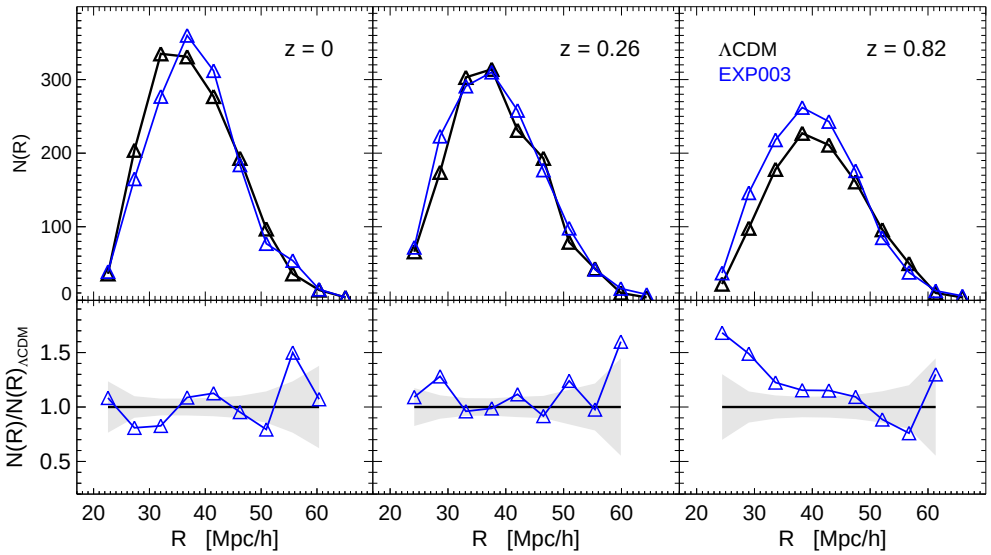

Figure 4.9: Same as fig. 4.8 but for different redshift.

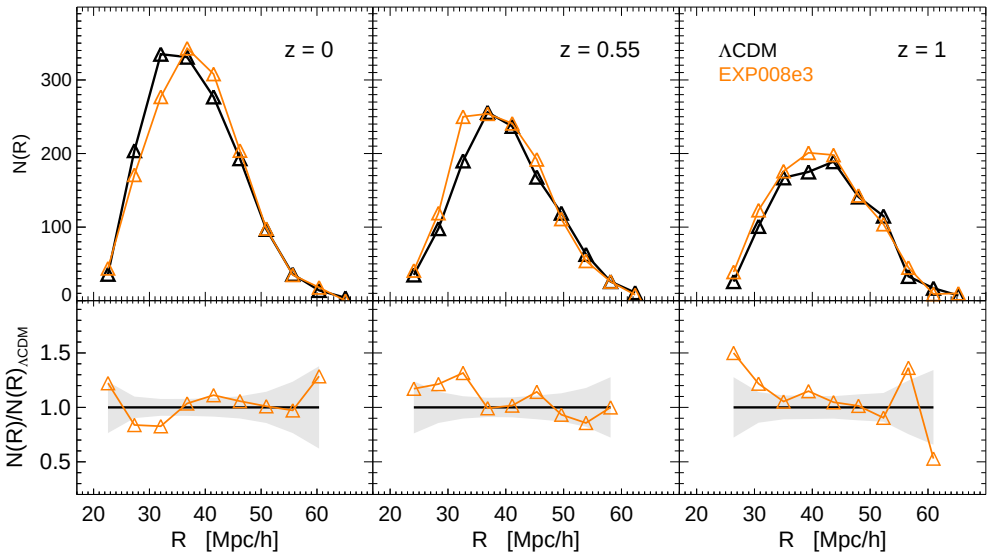

Figure 4.10: Same as fig. 4.6 but for the CoDECS simulations of EXP008e3 (orange).

tion Functions of the considered cDE models are all very similar to ΛCDM, at $z = 0.55$ and $z = 1.0$ cDE models all shows a larger portion of small voids than ΛCDM. In particular the EXP003 model at $z > 0.5$ shows a lack of voids with large radii and an excess of voids with small radii, but also model EXP002 shows the same feature at $z = 0.55$.

It is possible to take into consideration only the most extreme of the con-

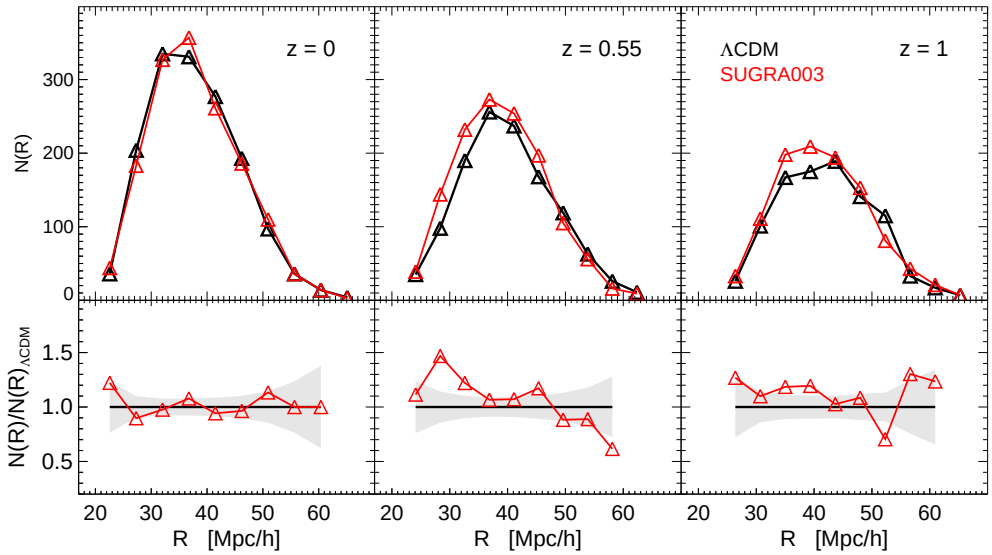

Figure 4.11: Same as fig. 4.6 but for the CoDECS simulations of SUGRA003 (red).

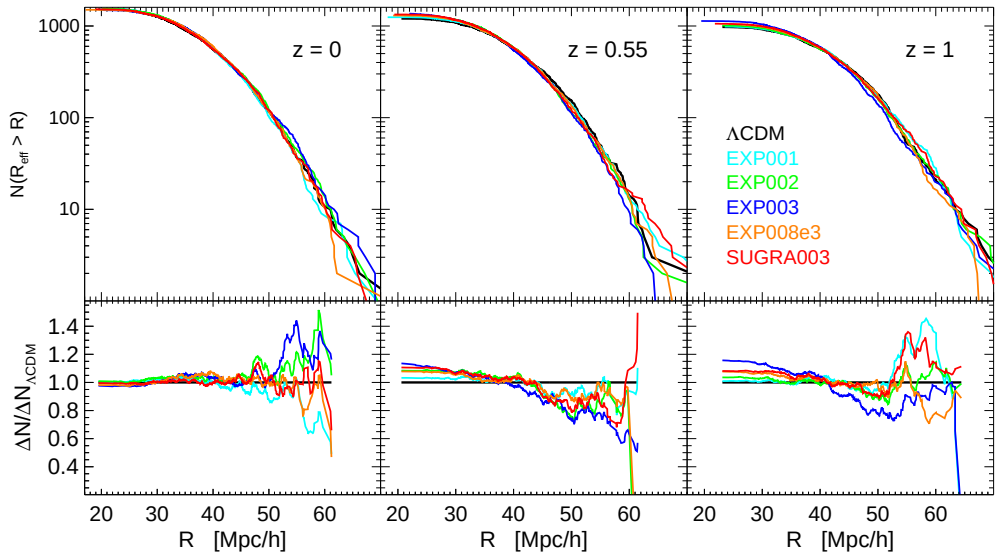

Figure 4.12: Cumulative Size Distribution Functions for the voids of all models included in the CoDECS suite at $z = 0, 0.55, 1.0$. In the top panels the distributions are compared, while in the bottom panels the ratios (calculated as explained in this section) between the distributions of the different models and ΛCDM are shown. The distributions do not show large differences at $z = 0$, but the excess of voids of small radii in the cDE models is confirmed.

sidered cDE models, EXP003, to better visualize the differences with ΛCDM produced by a strong coupling. We report the results using a logarithmic scale

on the y-axis (in fig. 4.13 and 4.14) and a linear scale in the y-axis (in fig. 4.15 and 4.16), to better display the behaviour at small radii.

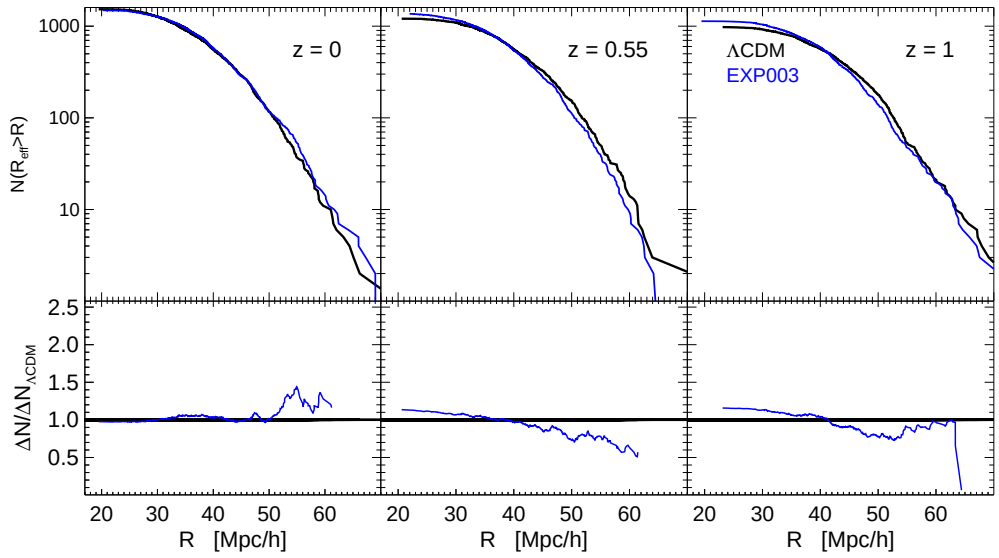

Figure 4.13: Comparison between Cumulative Size Distributions of voids in models EXP003 (blue) and ΛCDM of the CoDECS simulations. The top and bottom panels are organized as in fig. 4.12.

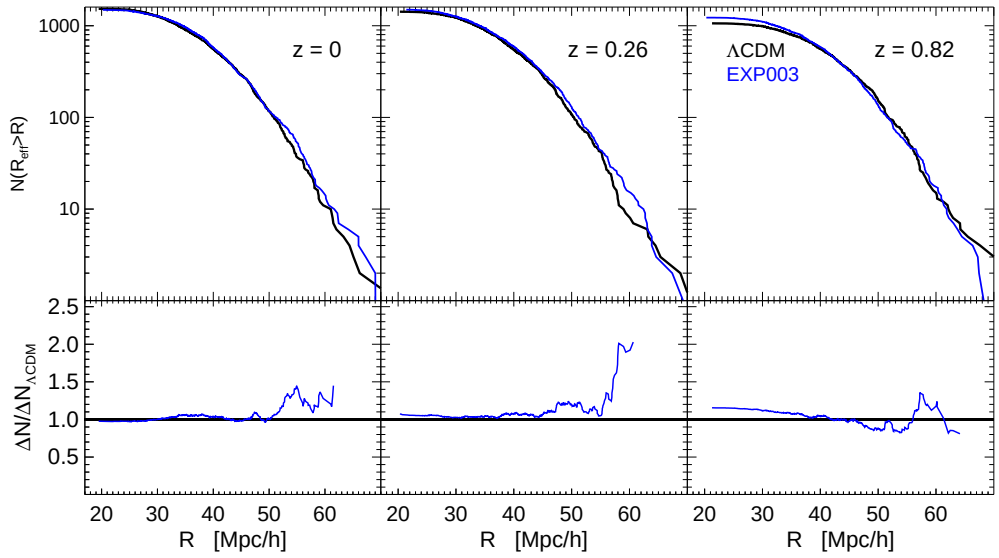

Figure 4.14: As fig. 4.14 but for $z = 0, 0.26, 0.82$.

The presence of a large number of voids with small radii in the considered cDE models at $z > 0.5$ can be explained as a consequence of a combination

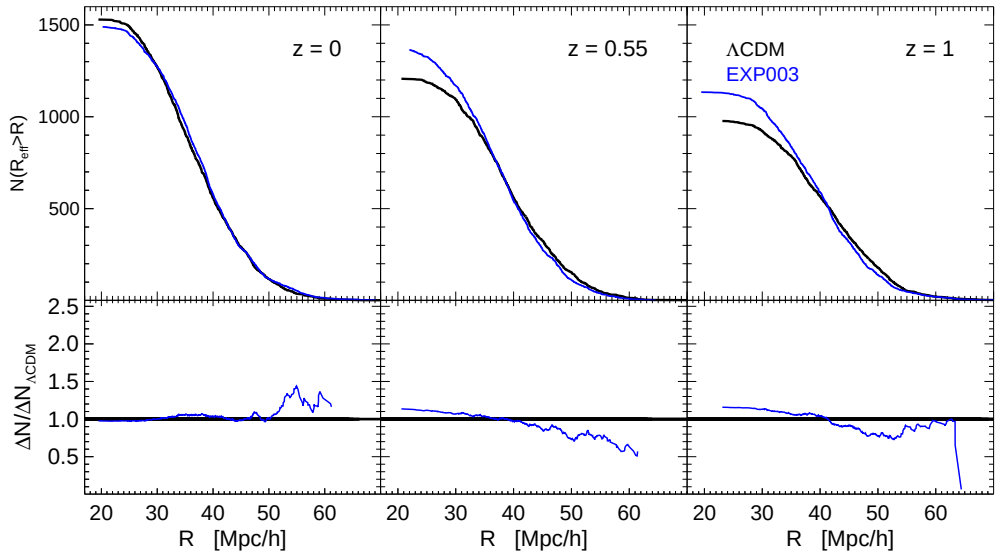

Figure 4.15: As fig. 4.13 but with a linear scale in the y-axis.

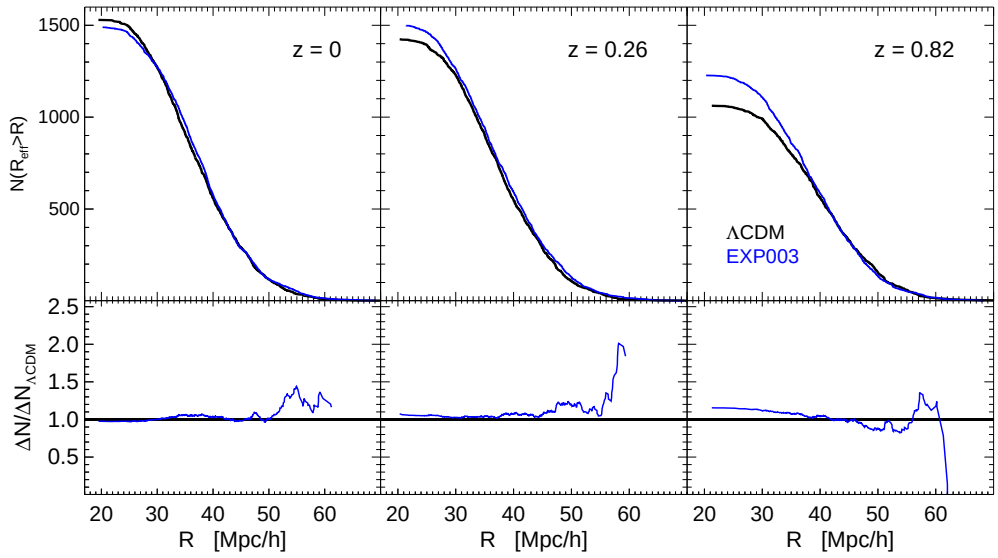

Figure 4.16: As fig.4.14, but with a linear scale in the y-axis.

of effects due to the different evolution of the perturbations in coupled DE scenario with respect to ΛCDM, summarized in eq. 2.23 (in which a "fifth force" term and a new friction term are included, see section 2.2.3), and different slopes of the *bias function* (that will be formally introduced soon) in the ΛCDM and coupled scenarios.

In the cDE picture, the contribution of the "Fifth force" causes density perturbations to grow more rapidly than density perturbation of ΛCDM.

This last statement is confirmed by values larger than ΛCDM of the cosmological parameter σ_8, which measures the amplitude of the linear power spectrum on the scale of $8Mpc/h$ (see ref. [40]).

The large values of σ_8 in cDE models are compensated by different evolution in redshift of the ***bias functions*** in Standard and coupled Quintessence scenarios (see ref. [42]), being the bias function of a single cosmological model defined as follows:

$$b^2(z) \equiv \frac{\xi_{halos}(z)}{\xi_{DM}(z)}\,, \tag{4.7}$$

where ξ_{halo} is the cDE correlation function of the halos and ξ_{DM} is the correlation function of the Dark Matter. In general

$$b_{cDE} \neq b_{\Lambda CDM} \tag{4.8}$$

being b_{cDE} the bias function in the cDE models and $b_{\Lambda CDM}$ the bias function of ΛCDM model; furthermore, in the cDE picture the bias function grows with redshift with a much softer trend than it does in the standard model.

To summarize, cDE models show values of σ_8 bigger than ΛCDM but present a slope of the bias function less steep than the one of the Standard Model.

The slow growth of the bias function at increasing redshifts in cDE scenarios allows halos to be spread around the density peaks in the density distribution of the Dark Matter so that the distribution of structures today is perfectly similar with the one that the Standard Model predicts and that we observe. Nevertheless, at high redshifts, the bias can determine some differences in cDE scenarios with respect to ΛCDM predictions, of which we have evidence thanks to differences in the clustering of structures (see ref. [42]). These differences must produce an effect also on voids properties that is what it is observed in the Size Distribution Function of model EXP003 (figs. 4.8, 4.9, 4.13 and 4.14) at high redshifts (i.e. $z > 0.55$) in particular, but also in the Size Distribution Function of model EXP002 at $z = 0.55$ (see figs. 4.7 and 4.12) and in general for cDE scenario at small radii for $z > 0.55$.

We probably observe this effect in the outcomes of model EXP003 in particular, because, as already pointed out, it presents the strongest value of coupling function β, see table 2.2.

Chapter 5

Stacked profiles

After having discussed the general properties of the Standard cosmological picture (chapter 1) and presented a possible alternative (i.e. the scalar field scenario, chapter 2) we are now investigating the differences between these alternative cosmological models using voids as a cosmological probe by means of the methods introduced in chapter 3. In chapter 4 the statistical properties of voids in different cosmological scenarios are discussed, reaching the conclusions that voids are homogeneously distribuited in the Universe and that their Size Distribution Functions present some differences only for the most extreme DE models under investigation.

In this chapter we start discussing the geometrical properties of voids by means of the comparison of their Stacked Density profiles, one of the possible methods that can be used to investigate the properties of voids. In fact, the stacked profiles of voids (which are the mean density profiles of voids with comparable size) provide an idea of how the internal structure of a void is designed.

5.1 Stacking procedure

Since our definition of voids is based on a spherical approximation (see eq. 3.3) it is possible to compute the spherically-averaged density profile of the voids included in our catalogues. Then, the stacked density profile is a mean density profile calculated among voids of comparable size (as presented in section 1.3).

The developed pipeline, which we have presented in section 3.3, computes for each void the density profiles, starting from the procedure explained at the end of section 3.2, under the spherical approximation. The profile is calculated considering spherical concentric shells of increasing radii. We choose to use 15 logarithmically equispaced radial shells starting from $0.2 \times R_{eff}$ up to $3 \times R_{eff}$. The lower limit is fixed in order to avoid considering radii which are comparable or smaller with respect to the resolution of the CoDECS sim-

ulation, i.e. $20Kpc/h$ (see ref. [47]), while the upper limit is chosen to be sufficiently large to recover a density equal to the mean density of the Universe, at large distances from the void center.

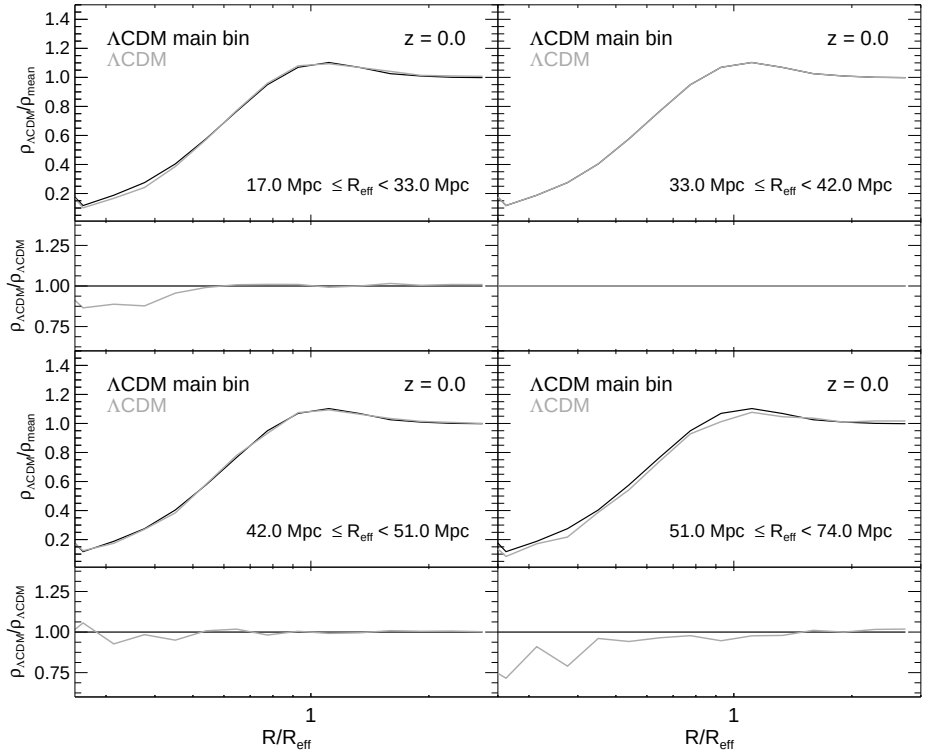

Figure 5.1: Comparison of the stacked profiles of the ΛCDM *main bin* (black) with all the other bins of ΛCDM model at $z = 0$. The top panels show the two density profiles, while the bottom panels displays the ratios between the two distributions. The profiles are all similar, as clearly visible in the bottom panels.

So, after having run the pipeline for all the models and all the redshifts taken into consideration, the density profile of every single void is known and it is only necessary to define a procedure which calculates the stacking profiles of voids.

Since the primary goal of this thesis work is to compare the differences among voids in different cosmological scenarios, we would like to calculate the stacked profiles (for a fixed model and at fixed redshift) so that many voids are included in each stacking bin. If this last requirement is fulfilled it will mean that, for every model, a good confidence on the profile shape will be reached and the comparison between different cosmological models will be statistically robust.

Looking at the *Differential Size Distributions Function* of all catalogues

(figs. from 4.6 to 4.11) it is possible to see that the largest fraction of voids in all the samples has a radius R_{eff} which is included in the range $30-35Mpc/h \lesssim R \lesssim 40-45Mpc/h$. This is a relevant information: the range $30-35Mpc/h \lesssim R \lesssim 40-45Mpc/h$ is going to be considered as the most important in our discussion.

After these general observations and once having stated our aim, let me present the stacking procedure, which starts as follows:

- only 4 bins over the range of void radii are defined so that a number of voids larger than ~ 200 is included in each bin;
- the ranges of the bins are $17Mpc/h \leq R < 33Mpc/h$, $33Mpc/h \leq R < 42Mpc/h$, $42Mpc/h \leq R < 51Mpc/h$, $51Mpc/h \leq R < 74Mpc/h$ for all the considered models and redshift;
- the stacked profile is calculated at fixed model, redshift and bin, as:

$$\overline{\rho}_i = \frac{1}{N}\sum_j^N \rho_i^j/\rho_{mean}$$

  where $\overline{\rho}_i$ is the mean density of the voids in the $i-th$ bin, N is the number of voids in the $i-th$ bin, ρ_i^j is the density of the $j-th$ void in the $i-th$ bin and ρ_{mean} is the mean density of the Box.

In fig. 5.1 the stacked profiles for the voids catalogue of ΛCDM are shown and all of the stacked profiles are compared with the stacked profile in the **main bin**, i.e. $33Mpc/h \leq R < 42Mpc/h$, which is the bin that includes the largest number of voids.

Firstly, it is possible to appreciate that the stacked density profiles are perfectly similar to the stacked density profiles found in the literature (see e.g. fig. 1.2 from ref. [46]). We would also like to stress that, while in ref. [46] the maximum of each single density profile is forced to be at $R = 1 \times R_{eff}$, so that in the stacked profile a compensative over-density is observed at $R = 1 \times R_{eff}$, in our stacked profiles this feature arises naturally without any further assumption.

Secondly, by the comparison of the profiles and of the ratios, no relevant differences are shown by the stacked profile in fig. 5.1. The bin $51Mpc/h \leq R < 74Mpc/h$ displays the largest deviations in the ratios with ΛCDM *main bin*. These are sensibly large only in the inner part of the void in which we observe a $\sim 25\%$ decrease: this might be significant and it possibly shows that the inner density of a void decreases when increasing the dimension of the void itself. Nevertheless, it has to be considered that this is the bin which includes the largest range of radii but in which the smallest number of voids is included so, statistically, it also presents the biggest uncertainty.

Therefore, it is possible to conclude that the stacked profiles of ΛCDM are all similar: the range of radii in which the stacking is computed does not affect its shape.

5.2 Evolution of the ΛCDM stacked profile

After having pointed out that the Stacked Profile of the *main bin* of the ΛCDM at $z = 0$ (from now on "SP-ΛCDM main bin") is representative of the general stacked density profile of the Standard Model at $z = 0$, it is possible to compare it with the stacked profiles calculated in the ΛCDM scenario at $z = 0.55$ and $z = 1.$, in order to investigate the possible differences in stacked profiles at different redshifts.

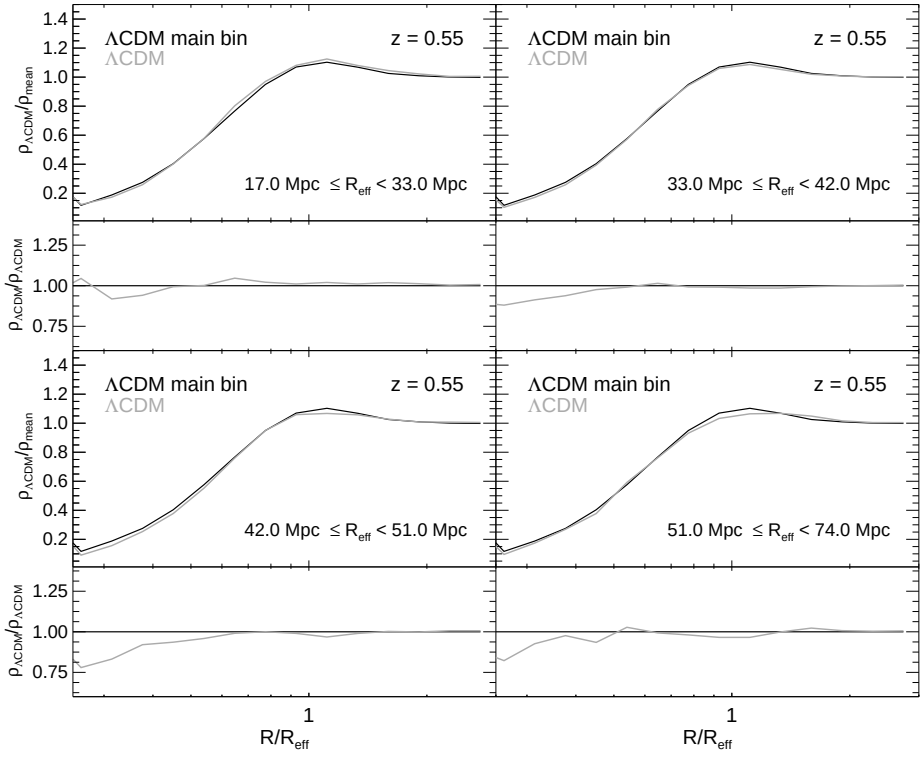

Figure 5.2: Same as figs. 5.1, but at $z = 0.55$.

In figs. 5.2 and 5.3 the comparison of the stacked void density profiles voids of the Standard Model catalogues at $z = 0.55$ and $z = 1.0$ with the SP-CDM main bin are reported, respectively.

Both the comparison of stacked profiles and their ratios, which are shown in the figures, do not display significative differences. The stacked profiles

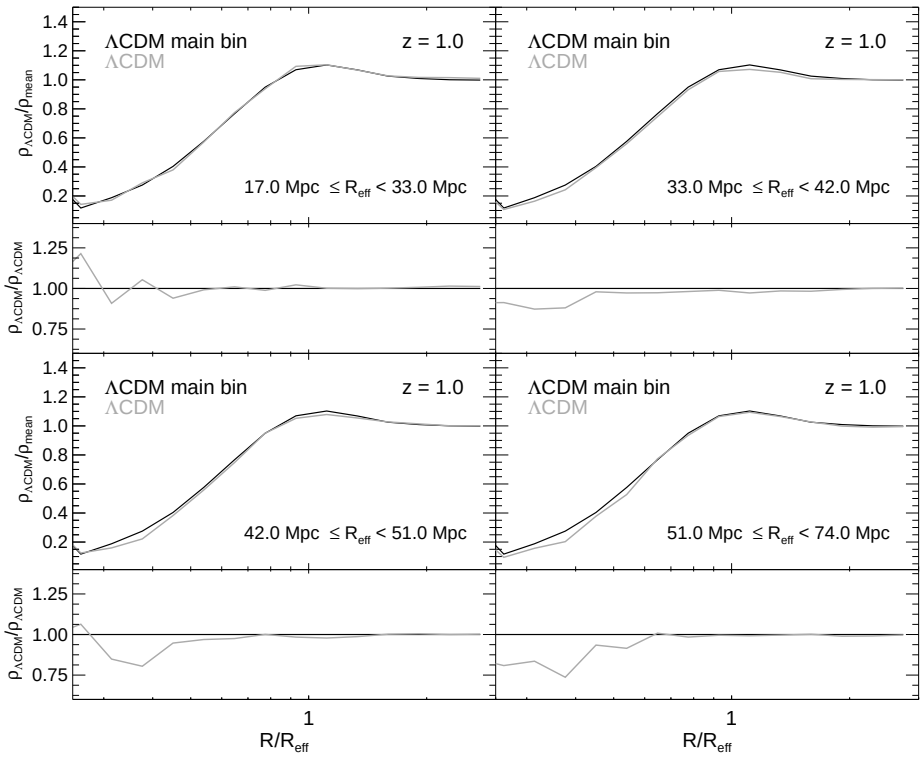

Figure 5.3: Same as fig. 5.1 but at $z = 1.0$

have all the same shape and in general no fundamental discrepancies are found. The only differences arise in the very inner part, which has generally a lower density for large voids.

It is then possible to conclude that *the evolution in redshift and the void size does not affect the shape of stacked density profiles of voids in the Standard Cosmological Model for* $R > R_{eff}/2$.

A similar result is presented in a recent work by Ricciardelli et al. (see ref. [56]) where the universality of voids profiles at $z < 0.15$ is strongly assessed by the investigation of two catalogues: the first one is extracted by observational data from the Sloan Digital Sky Survey (see ref. [45]), while the second one is built starting from the outcomes produced by a large cosmological simulation which was run with the code MASCLET. Ricciardelli et al. show that the stacked density (in the spherical approximation) from the simulation catalogues are fitted by the two-parameter law

$$\frac{\rho(< r)}{\rho_{eff}} = \left(\frac{r}{R_{eff}}\right)^{\alpha} \exp\left[\left(\frac{r}{R_{eff}}\right)^{\beta} - 1\right], \tag{5.1}$$

where $\rho(< r)$ is the density enclosed within the radial distance from the

void center r, ρ_{eff} is the density enclosed within the void effective radius R_{eff} and α and β are two free parameters. The fit is calculated using as tracers of the density field firstly the dark matter and then the gas. In both of the cases the stacked profiles are fitted by eq. 5.1 with similar best-fit parameters ($\alpha = 0.06$, $\beta = 1.76$ for the DM, and $\alpha = 0.01$, $\beta = 1.65$ for the gas), which is not surprising, since gas follows the density field created by the DM.

When comparing stacked profiles with different R_{eff}, Ricciardelli et al do not find any correlation of the parameters α and β with R_{eff}, at $z < 0.15$ so they argue that the profile is independent from the voids radius in the ΛCDM cosmology.

Our results show that the stacked density profile of voids in ΛCDM are also universal for $R > R_{eff}/2$, thereby confirming the general findings of Ricciardelli et al. Furthermore, in the next sections, we will extend this result to the considered cDE cosmological models.

5.3 Stacked profiles in different cosmological models

Based on the conclusion that was reached at the end of the previous section, it is possible to claim that SP-ΛCDM main bin is representative of the general stacked density profile of the Standard Model without being affected by the evolution with the redshift at $z \leq 1$ for $R > R_{eff}/2$.

We now compare the stacked profiles of all the cDE models included in the CoDECS suite at $z = 0$, $z = 0.55$, $z = 1.0$, with the stacked profiles of ΛCDM voids. We want to stress the possible discrepancy caused by different cosmologies, so we consider only the most densely populated bin (i.e. the *main bin*) only at a fixed redshift z.

In fig. 5.4 we report the ratios between the stacked profiles extracted from all of the cDE models included in the CoDECS suite and the stacked profile from the ΛCDM catalogue at redshift $z = 0$ considering the main bin only. At this redshift the largest differences are shown by models EXP001, EXP008e3 and SUGRA003 at $R \lesssim R_{eff}/2$. Models EXP002 and EXP003 show differences smaller than $\sim 5\%$. It is possible to observe that the profiles computed in cDE models all present a lower density in the very inner regions as compared to ΛCDM. The latter feature is not confirmed for all of the models at $z = 0.55$: in fact in fig. 5.5 it is possible to appreciate that models EXP002 and EXP008e3 clearly show stacked profiles with a larger inner density than ΛCDM, although all models except EXP002 show differences with respect to ΛCDM within the $\sim 5\%$.

The largest differences between the considered cDE models and ΛCDM are visible in fig. 5.6, where the comparison between stacked profile of voids is repeated as figs. 5.4 and 5.5 but at $z = 1$. In this figure all of the models show a deviation from ΛCDM of $\sim 10\%$. The differences generally arise in the inner regions of the profiles: while voids of models EXP003 and EXP008e3 show a larger inner density than voids of ΛCDM, the opposite result is found for EXP001, EXP002 and SUGRA003.

It is hard to define a clear trend among the considered cDE models, but it is possible to conclude that the largest differences in the stacked density profiles in cDE models with respect to the ΛCDM case are displayed at $z = 1.0$. Although the shape of the density profile is quite similar in all of the considered models, it seems that cosmology influences the inner density of cosmic voids in particular at higher redshifts. This feature should be further investigated in order to assess a possible trend in the discrepancy between the Standard Model and the cDE models.

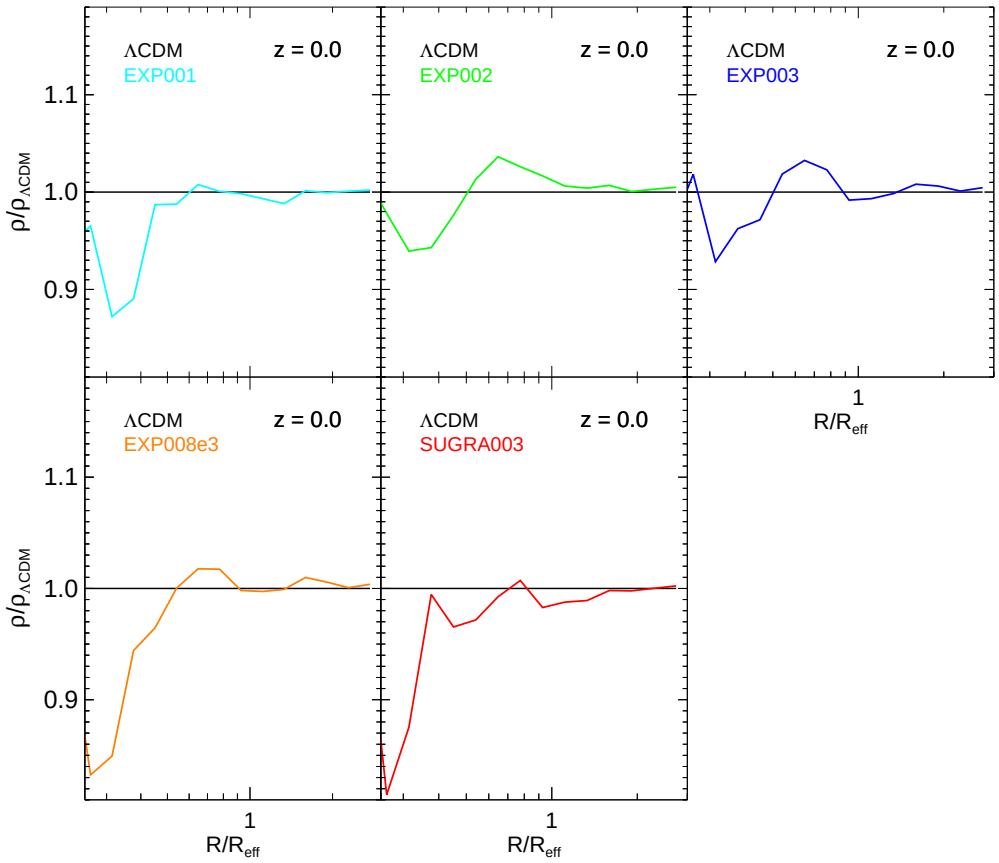

Figure 5.4: Ratios between the stacked density profiles of the cDE models included in the CoDECS suite and the ΛCDM profiles, both computed at $z = 0$ and in the most densely populated bin (i.e. voids with R_{eff} included in the range $33 - 42 Mpc/h$).

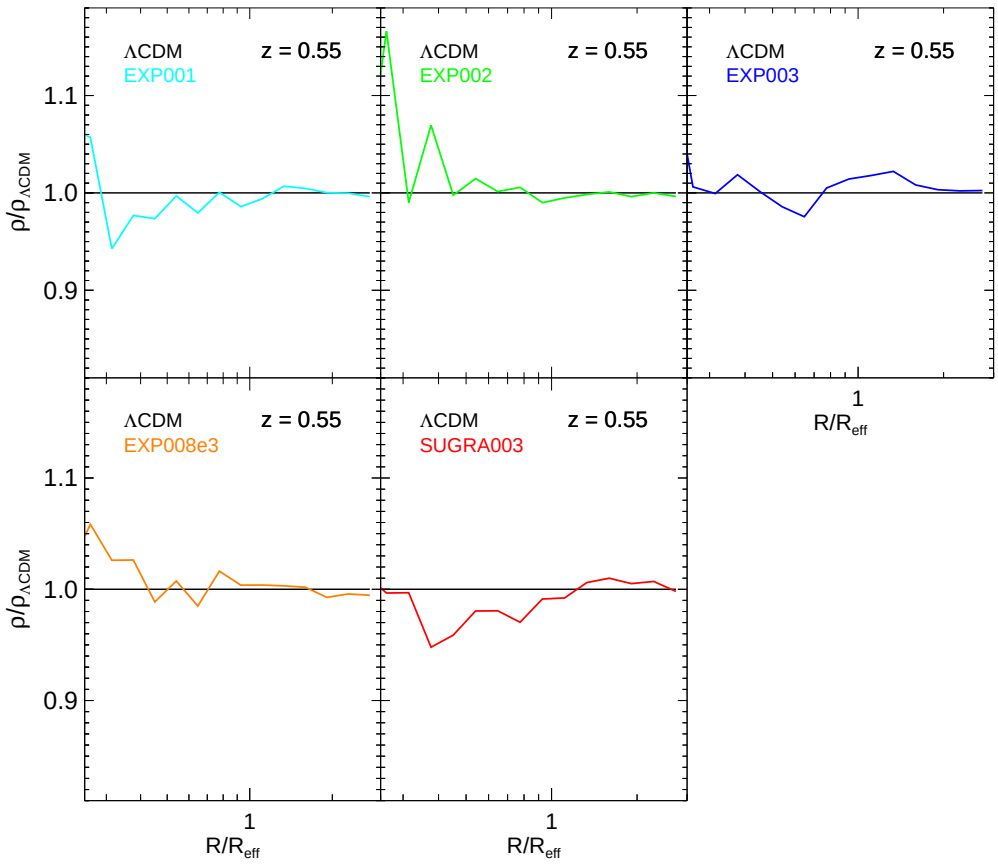

Figure 5.5: Same as fig. 5.4, but at $z = 0.55$.

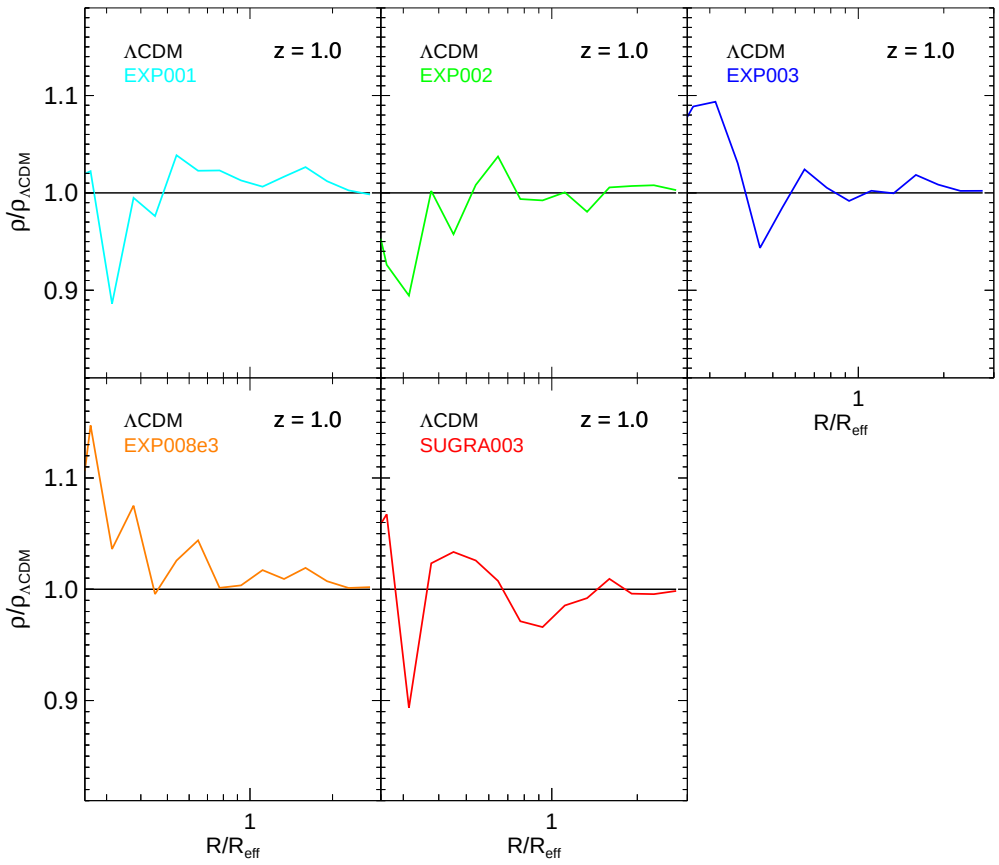

Figure 5.6: Same as fig. 5.4, but at $z = 1.0$.

5.4 Stacked profile evolution in different cosmologies

Looking at the Size Distribution of all models (figs. from 4.6 to 4.11) we see that the largest fraction of voids in each catalogue is included in the bin $33Mpc/h \leq R < 42Mpc/h$, so we used this bin to investigate the possible evolution with redshift of the stacked profiles of voids. We therefore investigate how the stacked profiles of cosmic voids evolve with redshift and if their evolution is influenced by the size of the considered voids. In figs. from 5.7 to 5.12 the comparison of stacked voids at fixed model is shown, in order to observe the effect due to evolution in redshift at different radii.

In fig. 5.7 we report the results for the ΛCDM model. The very inner region of the stacked profiles is particularly affected by the redshift evolution for all of the voids sizes, although the universality of cosmic voids profile is confirmed at $R > R_{eff}/2$. In particular we see that for voids with a radius R_{eff} within the intervals 33-$42Mpc/h$ and 42-$51Mpc/h$ (which are generally the most densely populated, see e.g. fig. 4.6) stacked profiles show at $z > 0.5$ (see the top right panels, and the bottom left panels) an inner density smaller than the one observed at $z = 0$. Nevertheless, an opposite feature is shown by the stacked profiles of voids with the smallest and the largest included radii (see the top left panels and the bottom right panels), which is what we expect due to the growth of the density perturbation.

In fig. 5.8 and 5.9 we report the results of the same analysis for the models EXP001 and EXP002. It is possible to observe that the universality of stacked profiles for $R > R_{eff}/2$ is confirm also for these models. Discrepancies of $\sim 10\%$ are shown in the very inner region of voids at redshift z higher than 0.5, but it is not possible to define a clear evolution of voids stacked profiles at increasing redshift for these models.

In fig. 5.10, we report the comparison of the evolution in redshift for voids of different size in the model EXP003. Despite the fact that for voids with a radius R_{eff} smaller than $51Mpc/h$ the discussion is perfectly similar to the models EXP002 and EXP003 (universality of the stacked profile of voids for $R > R_{eff}/2$ and slight differences in the very inner regions of voids), we observe that for the largest voids included in the catalogue ($R_{eff} > 51Mpc/h$) a significative difference ($\sim 50\%$) is shown by the stacked profiles of EXP003 at $z = 0.55$ (see bottom right panels) in the very inner regions.

Models EXP008e3 and SUGRA003 (in figs. 5.11 and 5.12, respectively) show the same feature found for the other models, but for R_{eff} within in $42-51Mpc/h$ we can see that at increasing redshift the voids have a decreasing central density, although, due to the growth of density perturbations, we would expect an opposite trend.

In conclusion, by the comparison of the redshift evolution of stacked profiles of cosmic voids with different sizes and in a fixed cosmological scenario we find that the largest differences arise in the inner region of cosmic voids, although the observed trend is not always clear. In general, we would expect the density of cosmic voids to decrease with the decrease of the redshift z but none of the considered models clearly shows this feature. Probably the bias $b(z)$ plays a fundamental role also in the evolution of the central den-

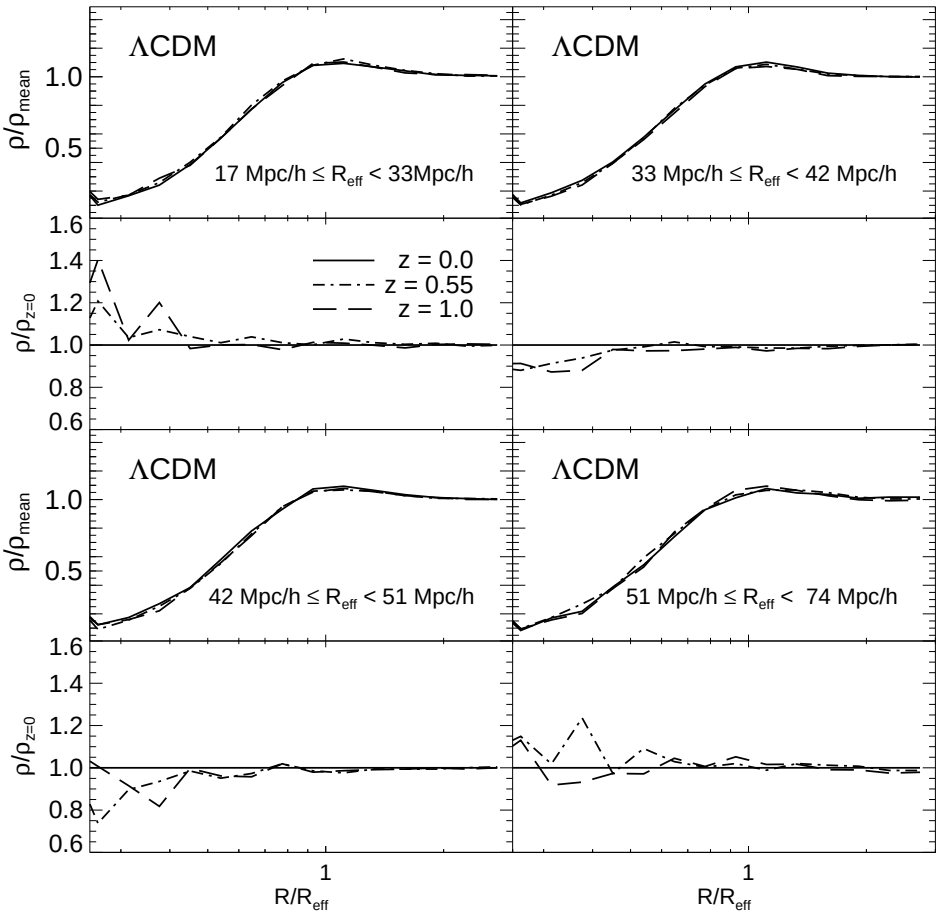

Figure 5.7: Comparison of the stacked density profiles of ΛCDM model at in different bins and redshift (top panels). The solid line represents the stacked profile at $z = 0$ while the dash-dotted line and the long-dashed line show the stacked profiles at $z = 0.55$ and $z = 1.0$ respectively. In the bottom panel we stress the differences between different evolutive stages by plotting the ratios between profiles at $z = 0.55$ and $z = 1.0$ and the stacked profile at $z = 0$.

sity of cosmic voids, and its interplay with the background evolution of the Universe leads to a non-trivial evolution of the central density of the stacked profiles. These properties should require further investigations.

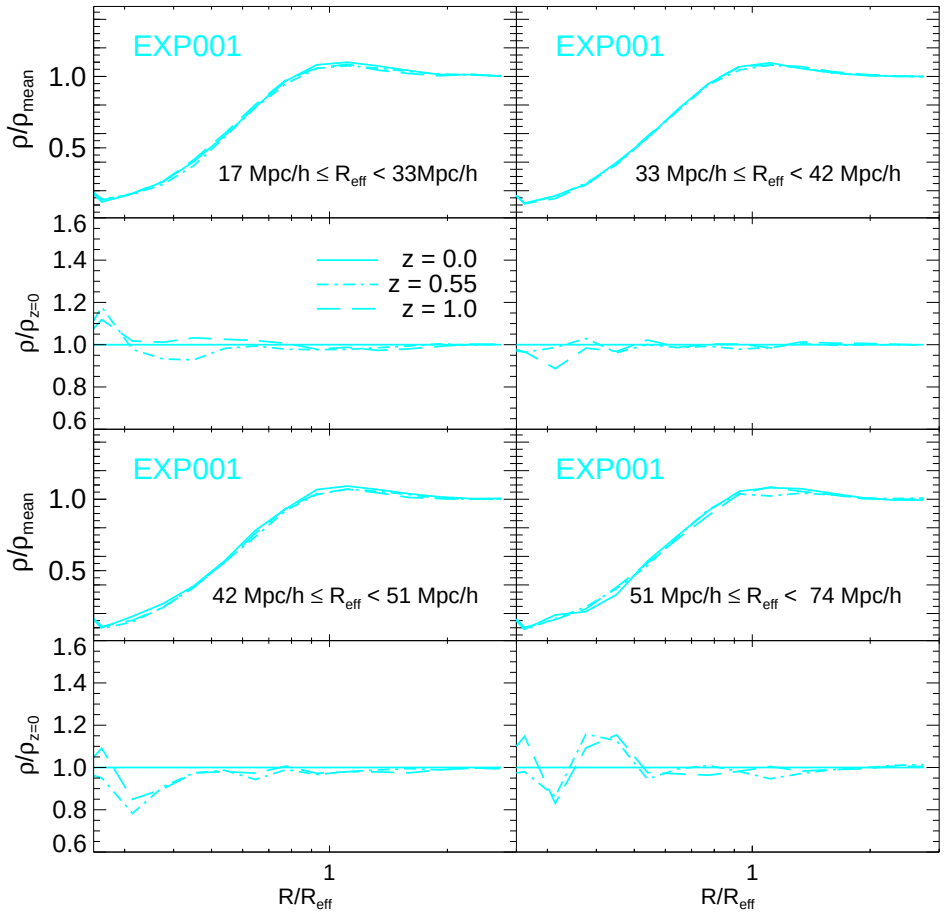

Figure 5.8: As fig. 5.7, but for model EXP001.

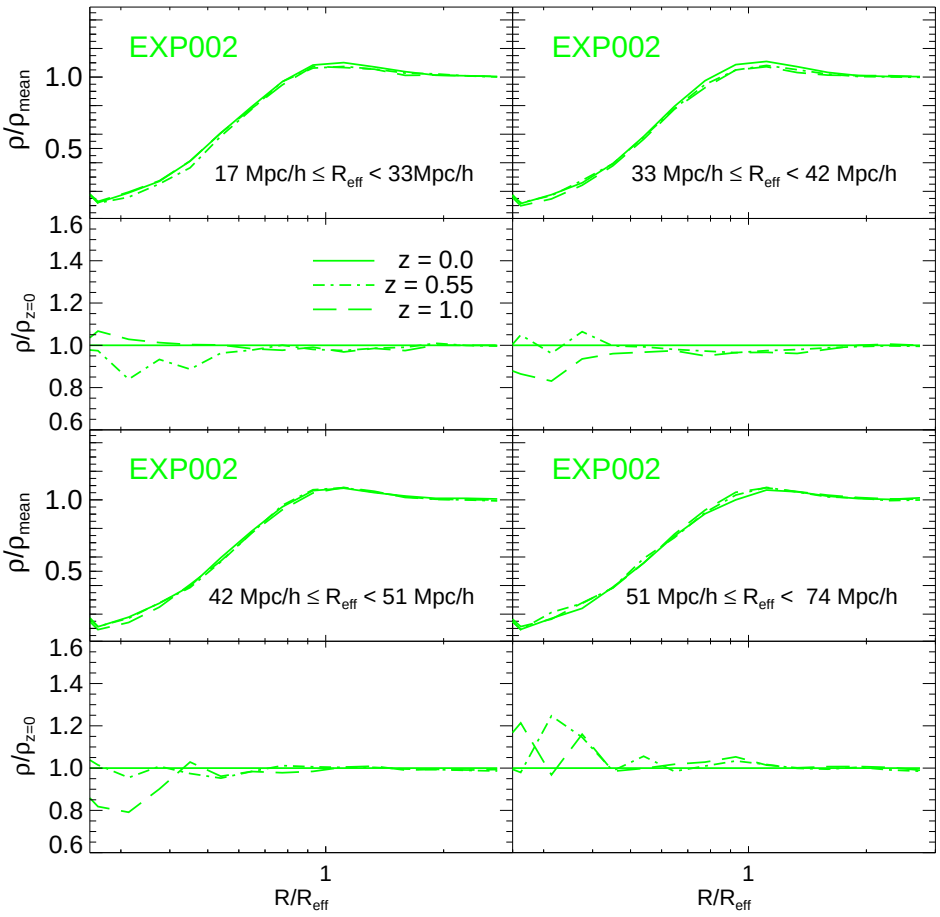

Figure 5.9: As fig. 5.7, but for model EXP002.

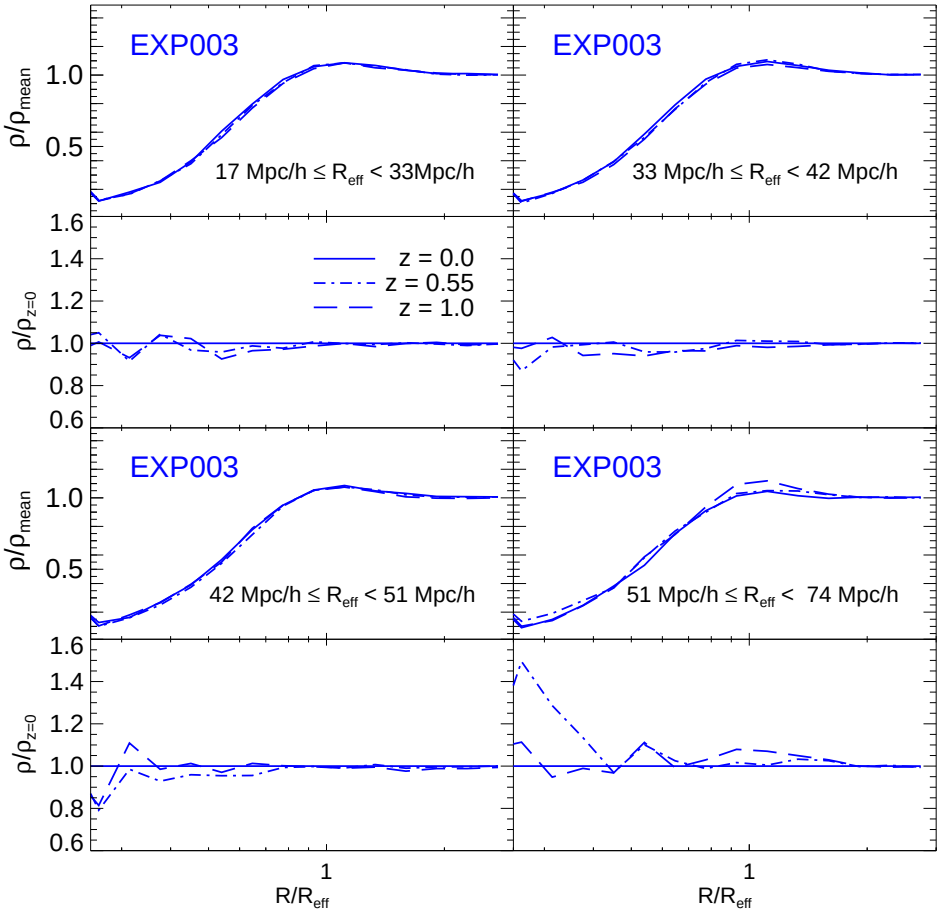

Figure 5.10: As fig. 5.7, but for model EXP003.

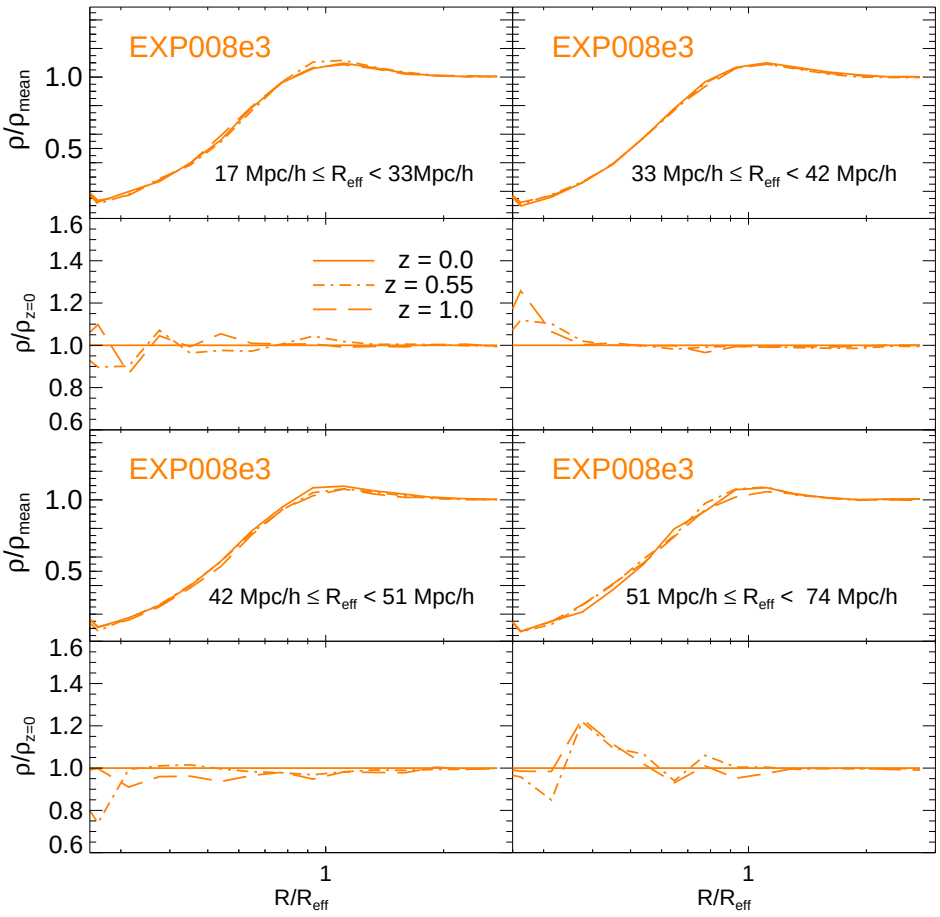

Figure 5.11: As fig. 5.7, but for model EXP008e3.

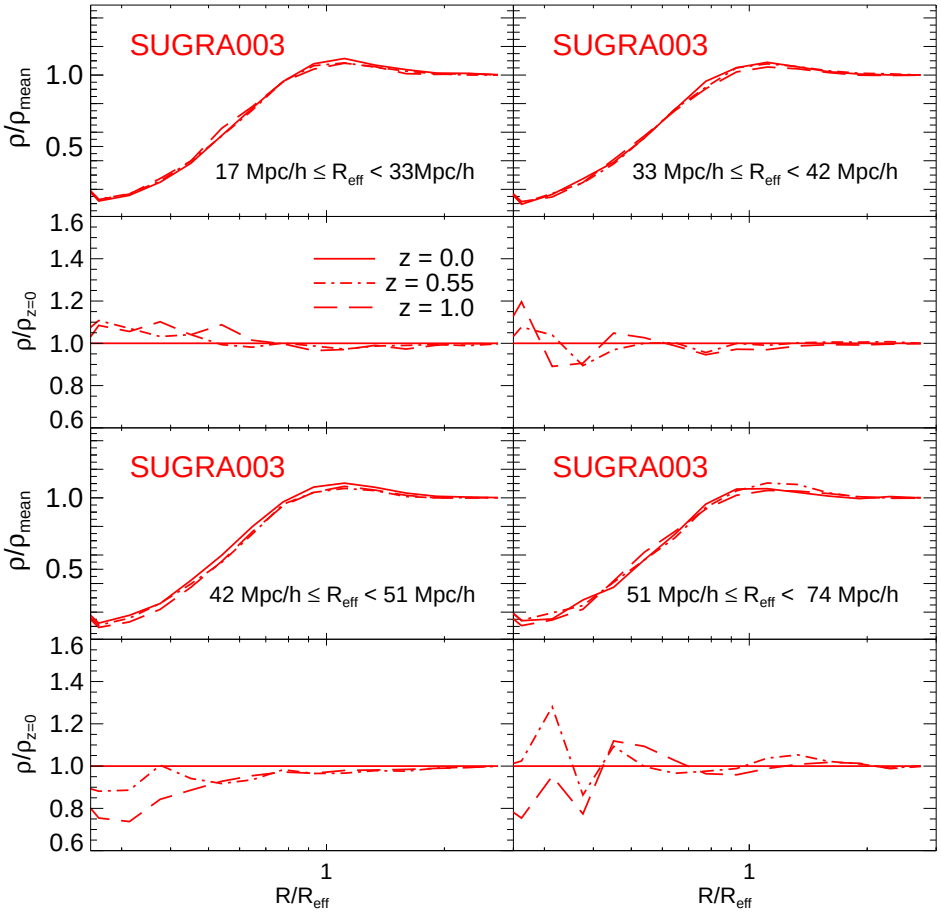

Figure 5.12: As fig. 5.7, but for model SUGRA003.

Chapter 6

Conclusions

In this chapter, after having recalled the scientific background in which this thesis work is set, we will summarize its major outcomes. Some possible way to extend the present work are also proposed.

The Scientific problem

The Standard Cosmological model is based on Einstein's field equations of General Relativity (eq. 1.5) and assumes two fundamental cornerstones (that are summarized by its acronym ΛCDM): the existence of a new type of massive non relativistic particles (the Cold Dark Matter, which provides the potential wells in which cosmic structures can form) and the presence of the Dark Energy (in the form of the Cosmological Constant Λ) which sources the accelerated expansion of the Universe we observe today (see chapter 1 and refs. [20], [21]).

Despite the fact that the ΛCDM model predicts correctly most of the features that are observed in our Universe, it leaves many questions unanswered and, as explained in section 2.1, shows several problems of self consistency.

One of the possible ways to address the problems of the Standard Cosmological Model is represented by the assumption of a form of dynamical Dark Energy, which is associated to a scalar field ϕ. As it is described in chapter 2, this last possibility is taken into consideration by the Quintessence scenario and the coupled Dark Energy theory, which both assume a dynamical form of DE but with different couplings to matter. In fact, while the Quintessence features a minimal coupling between ϕ and other fluid in the Universe, in the cDE a non-minimal coupling is explored (i.e. the scalar field is allowed to exchange energy with other components of the Universe).

One of the possible probes which can help us testing the properties of DE is represented by cosmic voids. The cosmic voids are large ($10 - 40\, Mpc/h$, see ref. [43]) under-dense regions in the Universe which originate from negative density fluctuations in the primordial density field (see ref [3]). Being almost devoided of matter, the dynamics of cosmic voids is supposed to be

dominated by DE, and they should be very sensitive to DE's nature. The appeal of cosmic voids is also related to their potential in probing cosmological parameters, since their general properties are found to be universal by many works (e.g. ref. [29], [54], [56]).

In the present work we have investigated the properties of cosmic voids in different cosmological models. Our interest in such objects is focused on their statistical and geometrical features by means of which we probe possible differences in voids properties between the standard ΛCDM and various scalar field cosmological scenarios. To reach this goal we use the pipeline created using the tools, the methods and the criteria described in chapter 3. We remember that our pipeline is based on the outputs produced by ZOBOV, a publicly available void-finding algorithm based on Voronoi Tesselletion. ZOBOV finds density minima and identifies voids of any shape around them. We decided to define voids as spheres centered in the volume-weighted center of mass of the tassels that ZOBOV includes in a void. The radius and the center of voids are calculated starting from ZOBOV's outputs, using eqs. 3.3, 3.4.

The results

The results of our analysis of the cosmic voids catalogues that we have built using our pipeline starting from the halo catalogs of the CoDECS simulations, are presented in chapters 4 and 5. We recall that CoDECS is the largest set of cosmological and hydrodynamical N-body simulations to date that feature a direct interaction between Dark Energy and matter (see section 2.3, and ref. [40]).

In chapter 4, we discussed the statistical properties of cosmic voids catalogues. The study of the Two-Point Correlation Function of cosmic voids shows that these objects are spread across the Universe with a homogeneous and isotropic distributions in the catalogues extracted from the simulations of the ΛCDM and cDE models at $z \leq 1.0$. This is a very interesting feature: primary, it confirms the Cosmological Principle (since we see that the distribution of voids in the Universe is homogeneous and isotropic at scales greater than $\sim 100 Mpc/h$). Secondly, since voids in our catalogues represent a class of spherical objects which have a homogeneous distribution in the Universe at different redshifts z, their typical dimensions can be used in order to characterize the history of the expansion of the Universe by means of an Alcock & Paczynski (see ref. [6]) test.

In 1979, Alcock and Paczynski (AP) proposed a cosmological test based on an hypothetical population of idealized spheres. The fundamental claim of such a test is the one that follows: because line-of-sight distances scale with the inverse Hubble parameter $H^{-1}(z)$ and transverse distances scale with the angular diameter distance $DA(z)$, their ratio measures the value of

the product $H(z)DA(z)$ and it encodes information about the expansion of the Universe. In practice, the AP test requires only statistical isotropy of the observed structures, which (from what we have pointed out in section 4.3) is the case of cosmic voids.

The AP test, 35 years ago, was devoted to investigate the possibility that $\Lambda \neq 0$ in Einstein's field equations (1.5), but now provides us with a new tool to distinguish a Cosmological Constant from alternative theories of dynamical Dark Energy. Recent works have used the AP test on stacked voids extracted from catalogues built on observational surveys with this purpose (see ref. [43], [44]), and our results validate the use of cosmic voids at $z < 1.0$ with this goal.

Going back to the results discussed in chapter 4, the comparison of the Size Distribution Functions (section 4.4) of voids belonging to different cosmological models shows a general agreement in the typical size of voids found in different cosmologies. The bulk of voids in our catalogues generally has a radius R_{eff} which is included in the range of $32Mpc/h \lesssim R_{eff} \lesssim 42Mpc/h$; all of the voids have a R_{eff} dimension in the range $\sim 17Mpc/h - 79Mpc/h$. In the comparison of the Size Distribution Functions among voids radii of the models included in the CoDECS suite, we also notice a peculiar behavior of the model EXP003, which is the only model that shows a visible discrepancy with respect to ΛCDM outcomes. In fact, at $z > 0.5$, EXP003 presents a fraction of voids with small radii larger than the one observed in the Standard Model. As already mentioned, this model presents the largest value of the coupling function β among the one included in the CoDECS set, and, as pointed out by Marulli et al. (ref. [42]), its bias function $b(z)$ shows an increase with respect to the redshift z which is slower than the bias function of the other cosmological model we considered. This means that the structures in EXP003 are spread around the density peaks of matter much more widely with respect to other models, and therefore we observe a larger fraction of small void than in ΛCDM at $z > 0.5$. This feature should be investigated deeply, and a first possibility is to run our pipeline for all models included in the CoDECS suite including new snapshots at $z > 0.55$.

In chapter 5, we presented the results of the stacking procedure by means of which we calculated the stacked density profile of cosmic voids in our catalogues. The comparison between all of the CoDECS models at all the considered redshifts remarkably shows the universality of stacked density profile of cosmic voids found in these models at $z \leq 1.0$. In the spherical approximation, profiles of cosmic voids show a large under-density next to the voids' center and a compensative over-density at $R \sim 1 \times R_{eff}$; the stacked profiles show the same qualitative shape of a individual profiles, although smoothed by the stacking procedure. The shape of the stacked density profiles for the models included in the CoDECS suite for redshift $z \leq 1$ and $R > R_{eff}/2$ is independent of the size of the void, evolution with redshift, and cosmology.

The same conclusion is reached by a recent work by Ricciardelli et al. (see

ref. [56]) in the context of the Standard Cosmological Model. In the work we have just mentioned, the universality of voids profiles is assessed by means of two voids catalogues. The former is built with the observational results from the Sloan Digital Sky Survey (see ref. [45]) while the latter is defined in a large cosmological simulation run by means of the hydrodynamical code *MASCLET* (see ref. [28]). Although some differences are shown between observational and numerical stacked voids profiles, being the former steeper than the latter, Ricciardelli at al. found a universality of voids density profile in the ΛCDM scenario at $z < 0.15$ in both of the cases. Many works based on cosmological simulations indicate that the density profile of voids is universal in the Standard Cosmological Model (see ref. [29] and [54]).

The general conclusion of this thesis work is that the properties of cosmic voids found in the spherical approximation using the halos as tracers of the underlyig field of the Universe are universal for the models included in the CoDECS suite at $z \leq 1$ and $R > R_{eff}/2$.

Follow-up analysis

The results that we have just presented in the last paragraph need further validation. There are many directions in which this thesis work can be extended.

In chapter 4 we reported that the Size Distribution Functions of the cosmic void are generally similar among different cosmologies and that only the model EXP003 at $0.5 < z \leq 1.0$ shows some differences with respect to ΛCDM. We wonder whether these properties stand also for $z > 1.0$ and a primary way to explore this possibility is to repeat our analysis on the CoDECS-halos results at $z > 1.0$.

Another possible way to point out differences in voids found in these models is to use matter distribution itself. In fact, in this thesis work we used the halos (for saving the computational time, but also because the position of the halos is associated to the position of the galaxies that we can observe in the sky) as tracers of the matter density but it is possible that more clear differences appear in the density distribution of standard or dark matter. Actually these differences naturally arise in cDE scenarios due to the modification of the evolution of perturbations (stated in eq. 2.23). Due to the combination of the effects caused by the fifth-force and by the additional friction term in cDE cosmologies the evolution of the density perturbations is faster than the one in ΛCDM. When looking at the distribution of collapsed halos, this effect is compensated by the fact that the bias function of cDE models has a slower growth in redshift with respect to ΛCDM, so that the distribution of the structures is more similar than the underlying matter distribution. We have evidence of this effect in voids properties only in EXP003 using halos as tracers of matter density.

We wonder whether or not a clear difference in the properties of voids

would be found using the distribution of the matter, and our analysis is worth being repeated in this case.

Finally, chapter 5 reports the robust evidence that the stacked voids profiles for our catalogues of voids are universal. This last result is reached under a spherical approximation. The assumption of a spherical shape for the voids is quite simple and is not perfectly supported by observations (e.g. see [38]): we will possibly go beyond it contemplating the fact that voids are ellipsoid of rotation. A repetition of the stacking procedure and a new study of voids statistical properties under this new assumption should definitely be considered.

Bibliography

[1] - Zur allgemeinen Relativitätstheorie, A. Einstein, 1915, Sitzungsberichte der Königlich Preußischen Akademie der Wissenschaften (Berlin), Seite 778-786.1915SPAW778E;

[2] - A relation between distance and radial velocity among extra–galactic nebulae, E. Hubble, 1929, Proc. Nat. Acad. Sci., 15:168–173;

[3] - Gravitational instability: An approximate theory for large density perturbations, Ya. B. Zeĺ dovich, 1970, A & A, 5, 84;

[4] - Gravitation and Cosmology: Principles and Applications of the General Theory of Relativity, S. Weiberg, 1972, John Wiley & Sons.

[5] -The Coma/A1367 supercluster and its environs, S.A. Gregory & L. A. Thompson, 1978, ApJ, 222, 784;

[6] - An evolution free test for non-zero cosmological constant, C. Alcock & B. Paczynski, 1979, Nature, 281, 358;

[7] - A million cubic megaparsec void in Bootes?, R. P. Kirshner, A. Jr Oemler, P. L. Schechter,S.A. Shectman, 1981, ApJ 248, L57-L60;

[8] - Fluctuations in the microwave background at intermediate angular scales, M. Melchiorri, B. O. Melchiorri, C. Ceccarelli, L. Pietranera, 1981, ApJ 250:L1-L4;

[9] - The evolution of voids in the expanding Universe, M.A. Hausman., D.W. Olson, B.D. Roth, 1983, ApJ, 270, 351;

[10] - Cosmology and the Fate of Dilatation Symmetry, C. Wetterich, 1988, Nucl. Phys., B302:668;

[11] - Cosmological Consequences of a Rolling Homogeneous Scalar Field, B. Ratra and P. J. E. Peebles, 1988, Phys. Rev., D37:3406;

[12] - The cosmological constant problem, S. Weinberg, 1989, Reviews of Modern Physics, Volume 61, Issue 1;

[13] -The Early Universe, Edward Kolb and Micheal Turner, Addison-Wesley Publishing Company, 1990;

[14] - Interpretation of the Cosmic Microwave Background radiation anisotropy detected by the COBE differential microwave radiometer, 1992 ApJ., 396:L13–L18;

[15] - The large-scale galaxy distribution in the Southern Sky Redshift Survey, S. Maurogordato, R. Schaeffer, L. N., da Costa, 1992, ApJ 390, 17;

[16] - Bias and variance of angular correlation function, S. D. Landy, A. S. Szalay, 1993, ApJ...412...64L;

[17] - The cosmon model for an asymptotically vaniching time-dependent cosmological "constant", C. Wetterich, 1995, Astron. Astrophys., 301:321–328;

[18] - The Las Campanas Redshift Survey, S. Shectamn, A. Stephen, S. Landy, A. Oemler, D. Tucker et al. 1996, ApJ 470, 172S;

[19] - How filaments of galaxies are woven into the cosmic web, J. R. Bond, L. Kofman, D. Pogosyan, 1996, Nature, 380, 603;

[20] - Observational Evidence from Supernovae for an Accelerating Universe and a Cosmological Constant. A. G. Riess at al, 1998, Astron. J., 116:1009–1038;

[21] - Measurements of Omega and Lambda from 42 High-Redshift Supernovae, S. Perlmutter et al, 1999 Astrophys. J., 517:565–586;

[22] - Quintessence and supergravity , P. Brax and J. Martin, 1999, Phys. Lett., B468:40–45.

[23] - Coupled quintessence, L. Amendola, Phys. Rev., D62, 043511;

[24] - Voids in the Las Campanas Redshift Survey versus cold dark matter models, V. Muller et al. , 2000, MNRAS, 318, 280;

[25] - The 2dF Galaxy Redshift Survey: spectra and redshifts, M. Colless, G. Dalton, et al., 2001, MNRAS, 328, 1039;

[26] - Dispense per il corso di Cosmologia Modulo A, G. Tormen, 2002;

[27] - Linear and nonlinear perturbations in dark energy models, L. Amendola, 2004, Phys. Rev., D69, 103524;

[28] - A new multidimensional adaptive mesh refinement hydro + gravity cosmological code, V. Quilis, 2004, MNRAS, 352, 1426;

[29] - Voids in a ΛCDM universe, J. Colberg et al, 2005, MNRAS, 360, 216;

[30] - Testing the Dark-Energy-Dominated Cosmology by the Solar-System Experiments , Yurii V. Dumin, 2008, Proceedings of the Eleventh Marcel Grossmann Meeting on General Relativity (edited by H.Kleinert, R.T.Jantzen and R.Ruffini). World Scientific, Singapore, pp.1752-1754;

[31] - VOBOZ: an almost-parameter-free halo-finding algorithm, M. Neyrinck et al, 2005, MNRAS, 356, 1222-1232;

[32] - ZOBOV: a parameter free void finding algorithm, Mark C. Neyrinck, 2008, MNRAS, 356, 1222;

[33] - ZOBOV Version 1.0 Documentation, M. Neyrinck, 2009;

[34] - Interaction between Dark Energy and Dark Matter - Dissertation der Facultät für Physik, M. Baldi, 2009,

[35] - Early dark energy at high redshifts: status and perspectives, J.Q. Xia & M. Viel, 2009, JCAP04(2009)002;

[36] - Clarifying the effects of interacting dark energy on linear and nonlinear structure formation processes, M. Baldi, 2010, MNRAS 000, 1–14 Printed, arXiv:1012.0002v2;

[37] - Time dependent coupling in the dark sector: from background evolution to non linear structure formation, M. Baldi, MNRAS 411.1077, 2011;

[38] - Cosmic Voids in Sloan Digital Sky Survey Data Release 7, D. C. Pan, M. S. Vogeley, F. Hoyle, Y. Choi, C. Park, 2011, arxiv: arXiv:1103.4156v2;

[39] - Environment and the Formation of Galaxies: 30 years later, R. van de Weygaert et al, 2011, ed. I. Ferraras & A. Pasquali, Astrophysics and Space Science Procedeengs (Berlin: Heildeberg: Springer Berlin Heildeberg);

[40] - The CoDECS project: a publicly available suite of cosmological N-Body simulations for interacting dark energy models, Marco Baldi, 2012, MNRAS 422, 1028–1044;

[41] - Precision Cosmography with Stacked Voids, G. Lavaux, B. Wandelt, 2012, ApJ 754, 109;

[42] - Clustering and redshift-space distortions in interacting dark energy cosmologies, F. Marulli, M. Baldi & L. Moscardini, 2012, arxiv:1110.3045v2;

[43] - A public void catalog from the SDSS DR galaxy redshift survey based on the watershed transform, P. M. Sutter, Guilhem Lavaux, Benjamin D. Wandelt, David H. Weinberg and Michael S. Warren, 2012;

[44] - A first application of the Alcock–Paczynski test to stacked cosmic voids - P. M. Sutter el al, 2012, ApJ, 761:187;

[45] - The Orientation of Disk Galaxies around Large Cosmic Voids, J. Varela et al, 2012, ApJ, 744, 82;

[46] - The Hierarchical Structure and Dynamics of Voids, M. A. Aragon-Calvo, A. S. Szalay, 2013, MNRAS, 428.3409A;

[47] - CoDECS (COupled Dark Energy Cosmological Simulation)'s guide, 2013, Marco Baldi;

[48] - Voids in modified gravity: excursion set predictions, J. Clampitt, Y. -C. Cai, B. Li, 2013, MNRAS [1212.2216];

[49] - Characterizing dark interactions with the halo mass accretion history and structural properties, C. Giocoli at al, 2013 , MNRAS Volume 434, Issue 4, p.2982-2998;

[50] - The abundance of voids and the excursion set formalism, E. Jennings et al, 2013, arxiv:1304.6087v2;

[51] - The power of the three-point correlation function: disentangling interacting dark energy cosmologies and estimating the halo bias, M. Moresco, 2013, submitted to MNRAS, arXiv: 1312.4530M;

[52] - Real-space density profile reconstruction of stacked voids, A. Pisani, G. Lavaux, P. M. Sutter, and B. D. Wandelt, 2013, arXiv:1306.3052v1 [astro-ph.CO];

[53] - The dark matter of galaxy void, P. M. Sutter, Guilhem Lavaux, Benjamin D. Wandelt, David H. Weinberg and Michael S. Warren, arXiv:1311.3301v1 [astro-ph.CO];

[54] - The structure of cosmic voids in a ΛCDM Universe, E. Ricciardelli et al, 2013, MNRAS, 434, 1192R;

[55] - A new geometrical approach to void statistic, M. C. Werner, 2013, arxiv: 1311:7209v1;

[56] - On the universality of void density profiles, E. Riccialrdelli, V. Quilis, J. Varela, 2014, arxiv:1402:2976v1.